

AD-A114 911

IOWA STATE UNIV AMES ENGINEERING RESEARCH INST

F/6 21/5

AERODYNAMICS OF ADVANCED AXIAL-FLOW TURBOMACHINERY, (U)

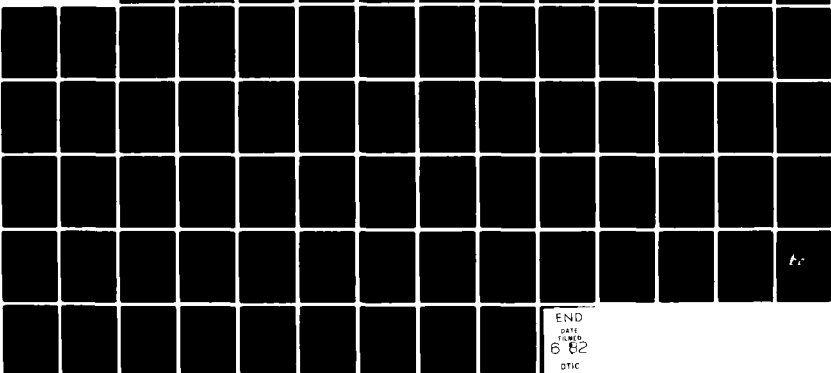
DEC 81 G K SEROVY, P KAVANAGH, T H OKIISHI AFOSR-80-0004

UNCLASSIFIED ISU-ERI-AMES-82108

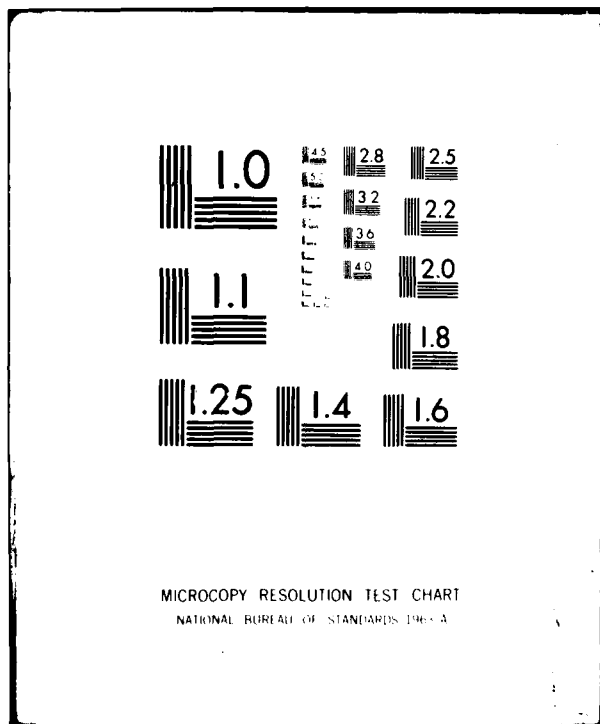
AFOSR-TR-82-0201

NL

1 of 1
G K SEROVY



END
101
6 82
DTIC



MICROCOPY RESOLUTION TEST CHART
NATIONAL BUREAU OF STANDARDS 1964 A

AER 114911

ADA 114911

Annual Report
1 October 1980 - 30 September 1981

AERODYNAMICS OF ADVANCED AXIAL-FLOW TURBOMACHINERY

APPROVED FOR PUBLIC RELEASE: DISTRIBUTION UNLIMITED

FILE COPY
TURBOMACHINERY
COMPONENTS RESEARCH PROGRAM

DTIC
REPRODUCED
MAY 2 1982
S-1

DISTRIBUTION STATEMENT A

Approved for public release;
Distribution Unlimited

REF ID: A624911
100-100000000000
100-100000000000

Qualified requestors may obtain additional copies from the
Defense Documentation Center; all others should apply
to the National Technical Information Service.

CONDITIONS OF REPRODUCTION

Reproduction, translation, publication, use and disposal in whole
or in part by or for the United States Government is permitted.

AIR FORCE OFFICE OF SCIENTIFIC RESEARCH / AFSC
NOTICE OF TRANSMISSION TO DDCI
This technical report has been reviewed and is
approved for public release by AFSC AFPL 13-12.
Distribution is unlimited.
MATTHEW J. KERPER
Chief, Technical Information Division

1/2

ENGINEERING RESEARCH

AERODYNAMICS OF ADVANCED AXIAL-FLOW TURBOMACHINERY

**Annual Report
1 October 1980 - 30 September 1981**

**George K. Serovy
Patrick Kavanagh
Theodore H. Okishi
December 1981**

**ISU-ERI-Ames-82108
TCRL-22
Projects 1489-1491**

**TURBOMACHINERY COMPONENTS RESEARCH LABORATORY
DEPARTMENT OF MECHANICAL ENGINEERING
ENGINEERING RESEARCH INSTITUTE
IOWA STATE UNIVERSITY AMES, IOWA 50011**

UNCLASSIFIED SECURITY CLASSIFICATION OF THIS PAGE (When Data Entered)

REPORT DOCUMENTATION PAGE		READ INSTRUCTIONS BEFORE COMPLETING FORM
1. REPORT NUMBER AFOSR-TR- 82 - 0201	2. GOVT ACCESSION NO. AD-A114 911	3. RECIPIENT'S CATALOG NUMBER
4. TITLE (and Subtitle) AERODYNAMICS OF ADVANCED AXIAL-FLOW TURBOMACHINERY	5. TYPE OF REPORT & PERIOD COVERED Annual Report 1 October 1980 - 30 September 1981	
7. AUTHOR(s) George K. Serovy, Patrick Kavanagh and Theodore H. Okiishi	6. PERFORMING ORG. REPORT NUMBER AFOSR-80-0004	
9. PERFORMING ORGANIZATION NAME AND ADDRESS Engineering Research Institute Iowa State University Ames, IA 50011	10. PROGRAM ELEMENT, PROJECT, TASK AREA & WORK UNIT NUMBERS 61102F 2307/A4	
11. CONTROLLING OFFICE NAME AND ADDRESS Air Force Office of Scientific Research /NA Bolling Air Force Base, DC 20332	12. REPORT DATE December 1981 82 PAGES	
14. MONITORING AGENCY NAME & ADDRESS (if different from Controlling Office)	15. SECURITY CLASS. (of this report) Unclassified	
16. DISTRIBUTION STATEMENT (of this Report) Approved for Public Release; Distribution Unlimited	15a. DECLASSIFICATION DOWNGRADING SCHEDULE	
17. DISTRIBUTION STATEMENT (of th. abstract entered in Block 20, if different from Report)		
18. SUPPLEMENTARY NOTES		
19. KEY WORDS (Continue on reverse side if necessary and identify by block number) axial-flow turbomachinery axial-flow compressor axial-flow turbine cascade flow	computational fluid mechanics turbomachine flow measurement	
20. ABSTRACT (Continue on reverse side if necessary and identify by block number) A multi-task research program on the aerodynamics of advanced axial-flow turbomachinery is continuing at Iowa State University. Program components are intended to result in direct contributions to the improvement of axial-flow fan, compressor, and turbine design procedures. A detailed experimental investigation of intrapassage flow in a large-scale, curved, rectangular cross section channel representative of turbomachinery passages is in progress. The use of stator geometry modification to improve stage performance through better	(continued)	

DD FORM 1 JAN 73 1473

82 05 24 142

UNCLASSIFIED

IV

20. Continued.

flow management is being investigated via laboratory tests of baseline and modified versions of a two-stage compressor. The relationships of differences in numerical values of linear cascade and compressor test results to nonsimilar test conditions is being studied. The penalties associated with the simplifications commonly incorporated in currently used boundary layer flow calculation codes when they are used to predict actual turbomachine flows are being identified. This annual report summarizes the progress achieved during the grant year and indicates the direction of each task for the immediate future.

Accession For	
NTIS GRA&I	<input checked="" type="checkbox"/>
DTIC TAB	<input type="checkbox"/>
Unannounced	<input type="checkbox"/>
Justification	
By _____	
Distribution/ _____	
Availability Codes	
Dist	Avail and/or Special
A	



TABLE OF CONTENTS

	<u>Page</u>
SECTION I. INTRODUCTION	1
SECTION II. STATUS OF THE RESEARCH PROGRAM	3
1. Task I: Experimental and Analytical Investigation of Intrapassage Flow in a Constant Mean Radius Rectangular Cross Section Passage Representative of Passages in Turbomachinery	5
2. Task II: Experimental Study of Stator Geometry Modifications for Improvement of Axial-Flow Compressor Aerodynamic Performance	23
3. Task III: Aerodynamics of Blade Surface Boundary Layer Development in Cascade Experiments in Compressor Operation--A Quantitative Evaluation	45
SECTION III. PUBLICATIONS	49
SECTION IV. PROGRAM PERSONNEL	51
SECTION V. INTERACTION WITH UNITED STATES AND FOREIGN GOVERNMENT AGENCIES AND INDUSTRY	53
SECTION VI. DISCOVERIES, INVENTIONS, AND SCIENTIFIC APPLICATIONS	55
SECTION VII. CONCLUDING REMARKS	57
REFERENCES	59
APPENDIX A. EXPERIMENTAL DATA TABULATION AND REDUCTION FOR PASSAGE TEST RIG (TASK I)	61
APPENDIX B. EXPLANATION OF HOW FLOW PARAMETERS DESCRIBING RESEARCH COMPRESSOR PERFORMANCE (TASK II) WERE OBTAINED	71
APPENDIX C. NOTES ON RESEARCH VISIT TO DFVLR (KOLN) AND ONERA (CHATILLON), 21-30 SEPTEMBER 1981	75

LIST OF FIGURES

	<u>Page</u>
1. Endwall inlet velocity profiles for the four test cases investigated.	7
2. Percent measured mass flow variation vs. traverse plane for Test Cases C and D.	10
3. Mass-averaged total pressure loss coefficient vs. traverse plane for the four test cases.	11
4. Local mass-weighted total pressure loss coefficient CPTM for selected traverse planes from Test Case D.	14
5. Local mass-weighted total pressure loss coefficient CPTM in Traverse Plane No. 12 for the four test cases.	19
6. Various representations of total pressure loss coefficient in Traverse Plane No. 10 for Test Case C.	22
7. Meridional plane view of new blading.	24
8. Representative baseline and modified compressor rotor blade sections.	25
9. Representative baseline configuration stator blade sections.	26
10. Overall performance data for baseline and modified compressors.	27
11. Blade-to-blade distribution of time-average total-head data for flow behind the first- and second-stage rotors of the baseline compressor for flow coefficient = 0.587.	28
12. Blade-to-blade distribution of time-average total-head data for flow behind the first- and second-stage stators of the baseline compressor for flow coefficient = 0.587.	31
13. Comparisons of circumferential-mean data for flow behind the first- and second-stage rotors of the baseline compressor for flow coefficient = 0.587.	35
14. Comparisons of circumferential-mean data for flow behind the first- and second-stage stators of the baseline compressor for flow coefficient = 0.587.	38
15. Representative modified stator blade sections.	41

LIST OF FIGURES (cont.)

	<u>Page</u>
A1. Listing of five-hole probe data files.	62
A2. Listing of Kiel probe data files.	64
A3. Listing of reduced pressure coefficients for suction and pressure sidewalls.	65
A4. Listing of reduced pressure coefficients for bottom end-wall.	65
A5. Listing of reduced pressure coefficients for top endwall.	65
A6. Schematic of test section showing dimensions, traverse plane identification and coordinate system convention.	66

LIST OF TABLES

	<u>Page</u>
1. Summary of the inlet endwall boundary layer characteristics and traverse plane measurements made.	8

SECTION I. INTRODUCTION

The Turbomachinery Components Research Program at Iowa State University is involved in experimental and analytical fluid mechanics research projects covering a wide range of turbomachinery applications. These projects have been supported for some 25 years by government agencies, including the National Aeronautics and Space Administration (NASA), the United States Air Force Office of Scientific Research (USAF/AFOSR), the United States Air Force Aero Propulsion Laboratory (USAF/AFAPL), the Naval Air Systems Command, the National Science Foundation (NSF), and by various industrial concerns. The present research project involving aerodynamic studies of advanced axial-flow turbomachinery, as discussed in this report, was initiated in October 1978 under funding through AFOSR Contract F49620-79-C-0002. Currently, three individual tasks are identified in the overall research effort. As such, these involve an analysis of secondary flow and associated losses in blade passages, modifications of stator blade row geometries to control end-wall flows in compressors for improved performance, and an evaluation of recent boundary layer and wake computational methods based on comparisons of experimental cascade and rotational blade row data. These tasks are being continued and extended at the present time under provisions of ~~AFOR~~ AFOR-81-0004

Summaries of the results achieved in the three individual research tasks are included in the following section.

SECTION II. STATUS OF THE RESEARCH PROGRAM

Each of the three tasks in the research program is discussed in this section. Task I originated in internally-supported work at Iowa State University and is based on earlier analyses carried out with support from the Pratt and Whitney Group of the United Technologies Corporation. The results are providing further knowledge of the complex, three-dimensional internal flows involved in curved channels, and they will be used to assess the usefulness of computer codes purported to model similar flow situations. Task II evolved from discussions with Dr. Arthur J. Wennerstrom of AFAPL and is intended to result in fundamental design data that will be usable in future high efficiency multi-stage axial-flow compressor development. Task III is based on concerns that arose previously while pursuing research on deviation angle prediction sponsored by the Air Force (AFAPL, AFOSR) and NASA and that are considered important by members of AGARD/PEP Working Group 12. This task is expected to result in suggestions for future research and improvements in computer code use.

1. TASK I: EXPERIMENTAL AND ANALYTICAL INVESTIGATION OF INTRAPASSAGE FLOW IN A CONSTANT MEAN RADIUS RECTANGULAR CROSS SECTION PASSAGE REPRESENTATIVE OF PASSAGES IN TURBOMACHINERY

1.1. Introduction

The requirements of high-performance modern aircraft gas turbines demand high-pressure turbine components with low aspect ratio blade rows and low-pressure turbines with strongly divergent endwalls. The endwall and secondary flows in these cases influence the flow throughout the entire passage and contribute a major portion of the total pressure loss and airfoil unloading effects encountered. It has been recognized for some time that extensive additional information is required to help supplement conventional turbine cascade design systems with, ultimately, three-dimensional flow analyses forming the basis for such design systems. For this reason, a detailed investigation of intrapassage flow in a large-scale, curved rectangular cross section passage representative of turbomachinery passages was undertaken. The experimental results thus obtained will provide further knowledge of the complex internal flow structure involved, identify secondary loss contributions, and aid in evaluating and checking theoretical flow analyses for three-dimensional cascade geometries as they are developed in future work.

1.2. Experimental Facility and Passage Test Rig

In the subject curved passage, significant secondary flow can occur without additional complications of cascade leading and trailing edge effects and tip clearance flows. Also with low-speed, incompressible flow testing, the essential details of the three-dimensional flow field are present. In the present investigation, the test passage consists of

a 90-degree bend of constant mean radius followed by a straight discharge section. The geometry of the test passage and probe traverse stations are summarized in Appendix A along with a description of data files collected, parameter definitions, and data reduction procedures. References 1 and 2 provide a complete description of the test passage and associated test rig components and data acquisition system.

1.3. Summary of Results

Figure 1 shows four different inlet velocity profiles used to investigate effects of changes in inlet endwall boundary layer characteristics on secondary flow and losses in the test passage. Curved wire-mesh screens were inserted into the boundary layer generator section upstream of the test passage to produce the test velocity profiles. By these means, a variety of controlled, two-dimensional and symmetrical velocity profiles could be generated between the upper and lower endwalls at the inlet to the passage. Measurements of the endwall boundary layers were made with a boundary layer probe (0.66 mm O.D.) at a station 3.8 cm upstream of the start of the bend. The boundary layer measurements are summarized in Table 1. Also shown in Table 1 are the traverse planes measured and the probe type used in each test case.

A critical factor influencing secondary flow in a curved passage, along with the amount of turning and the contraction of the passage, is the momentum thickness of the inlet endwall boundary layer. The secondary flow generated is characterized and is initiated by a crossflow directed from the outside towards the inside of the bend across either endwall. As the flow along the endwall enters the curved passage and

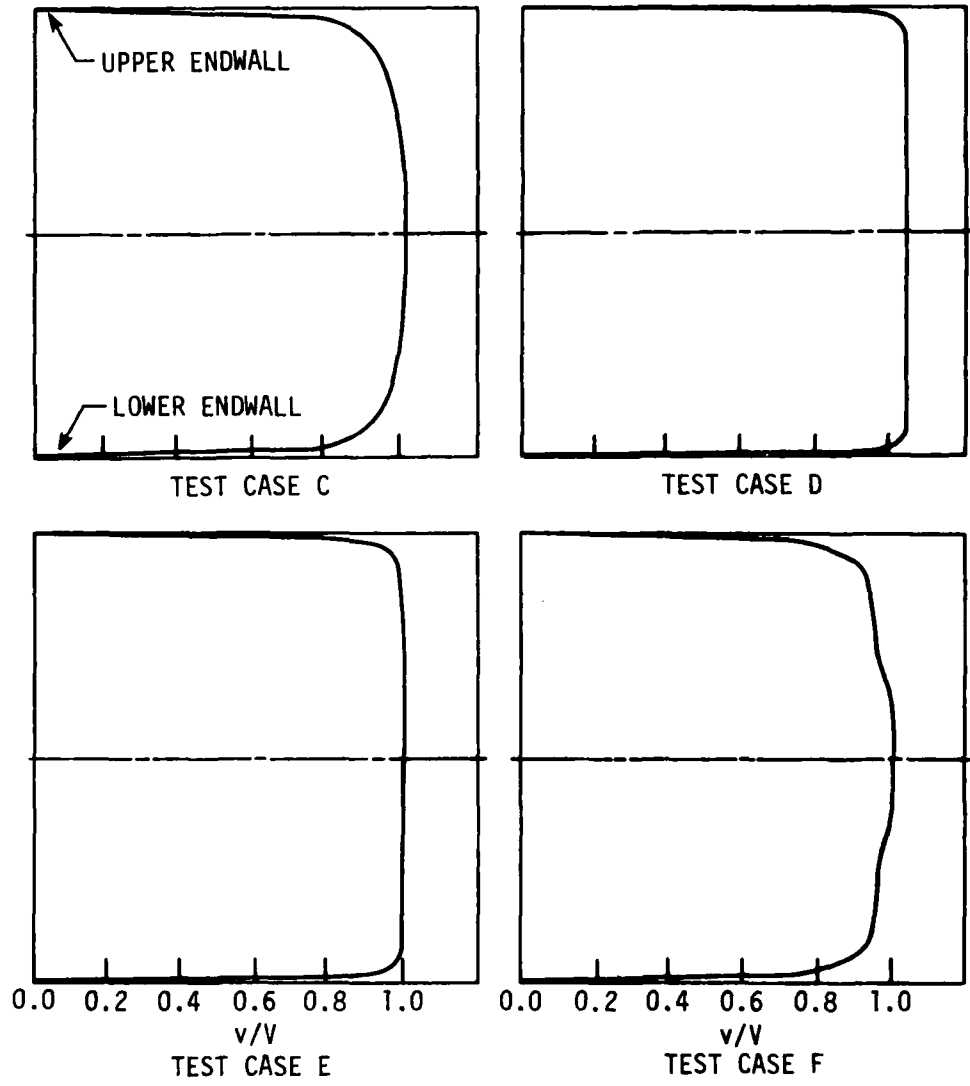


Fig. 1. Endwall inlet velocity profiles for the four test cases investigated.

Table 1. Summary of inlet endwall boundary layer characteristics and traverse plane measurements made.

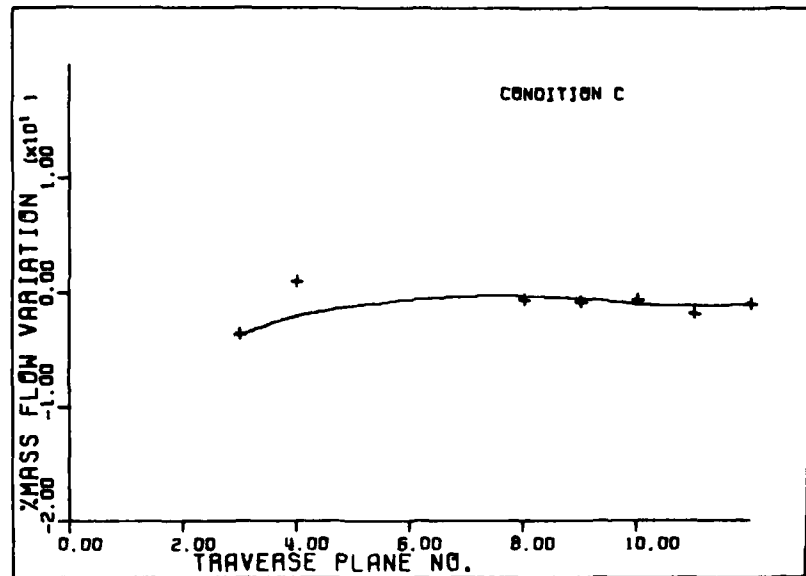
Test Case	Boundary Layer Thickness, in(cm)	Displacement Thickness, δ^* , in(cm)	Momentum Thickness, θ^* , in(cm)	Traverse Plane Probe Used	Traverse Planes Measured
C	4.11(10.4)	0.338(0.86)	0.278(0.71)	5-hole	3,4,5,8,9,10,11,12
D	0.91(2.31)	0.083(0.21)	0.072(0.18)	5-hole	1-12
E	1.51(3.84)	0.161(0.41)	0.127(0.32)	Kiel	3,4,5,6,7,9,11,12
F	5.01(12.7)	0.413(1.05)	0.352(0.89)	Kiel	3,4,5,6,7,9,12

encounters cross passage pressure gradients, it is swept into the corner formed by the endwall and suction sidewall. The strength of the cross flow and resultant secondary flow losses for a given passage configuration may be correlated with the extent of low-momentum flow present in the inlet velocity profile. An objective of this testing is to investigate such a correlation.

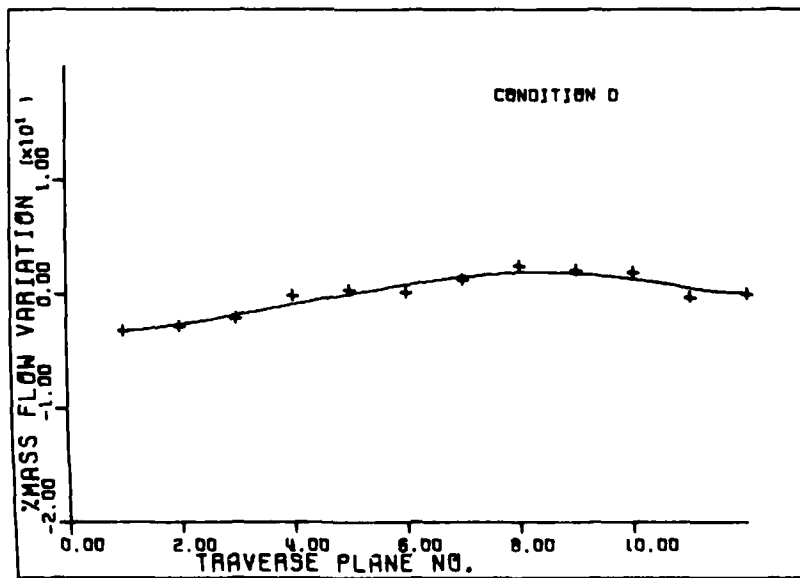
The process of the cross flow is complicated, however, by the three-dimensionality of the endwall flow which tends to "unload" the cross passage pressure gradients as the endwall is approached from the midspan position. After the cross flow is initiated, it proceeds to interact with the suction sidewall boundary layer, as evidenced by flow visualization, and a separation line along the suction sidewall is created with a consequent passage vortex formed.

Figures 2 through 5 present results of the detailed intrapassage measurements obtained in several traverse planes using the five-hole probe and Kiel probe. The percentage variation in mass flow between traverse planes as determined from five-hole probe measurements are presented in Figure 2 for test cases C and D. The mass flow for each traverse plane was calculated using the through-flow velocity component (V_y), which was made independent of inlet q by dividing by \sqrt{q} . These mass flow comparisons were carried out to assess the accuracy of the five-hole probe measurements in the traverse planes. As can be seen in Figure 2, the mass flow variations obtained in either case lie within $\pm 3\%$, indicating good consistency in the probe measurements.

Figure 3 presents the passage mass-averaged total pressure loss coefficient CPT for each traverse plane measured in the four test cases.

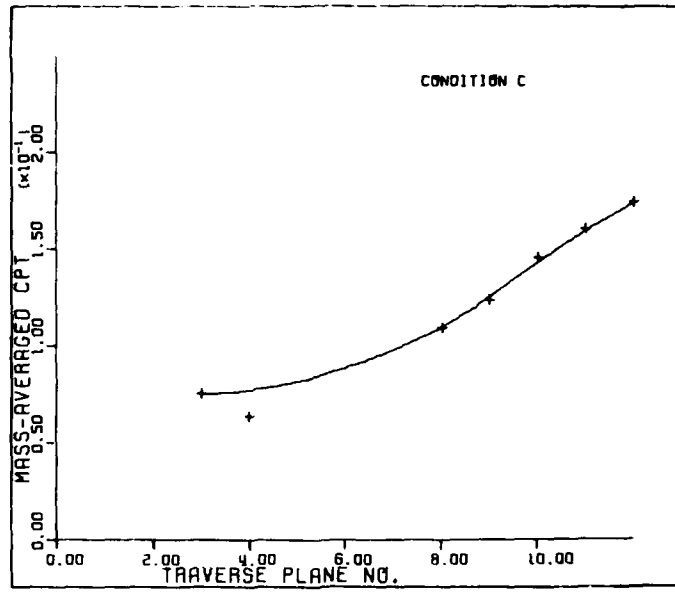


TEST CASE C

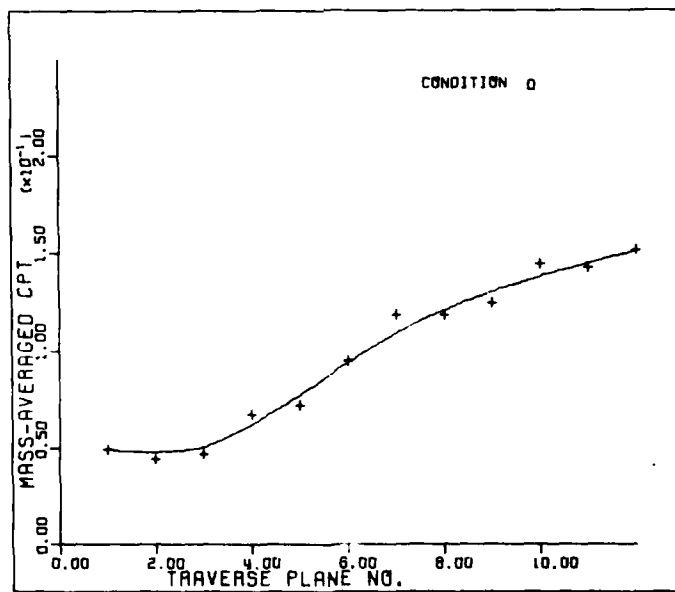


TEST CASE D

Fig. 2. Percent measured mass flow variation vs. traverse plane for Test Cases C and D.

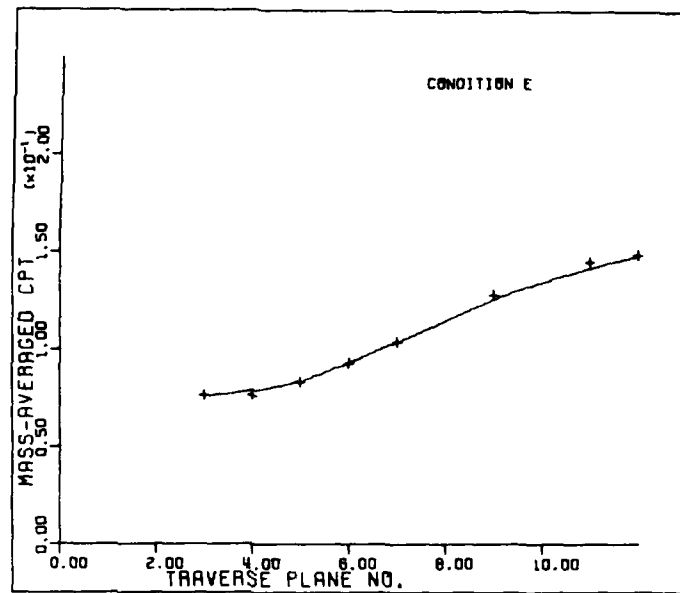


TEST CASE C

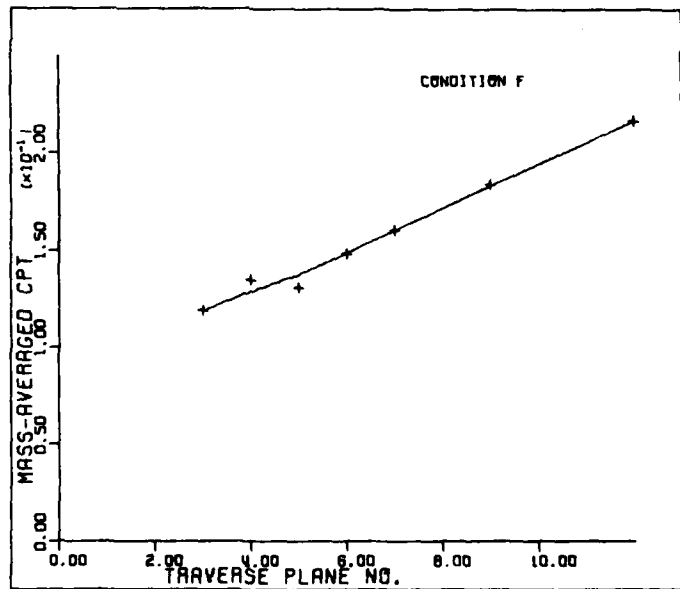


TEST CASE D

Fig. 3. Mass-averaged total pressure loss coefficient vs. traverse plane for the four test cases.



TEST CASE E



TEST CASE F

Fig. 3. (concluded).

These losses constitute the complete passage loss, including that of the inlet flow, and are computed through integration of the local mass-weighted total pressure loss coefficient, CPTM. This latter coefficient is obtained by weighting the local CPT by the fraction of the total mass flow associated with it. Flow angle data obtained from five-hole probe measurements are used in determining the local mass flows for the mass-weighting procedure for total pressure loss coefficient. In the case of Kiel probe data, the same weighting procedures were used. The same flow angles from five-hole probe measurements were assumed based on similar flow patterns observed in the four test cases. The different behavior of the loss coefficient through the passage is noted for the four test cases. In Test Case F ($\theta_{inlet}^* = 0.89$ cm) CPT is appreciably greater throughout the passage than for the other three cases, with values continuing to increase at a uniform rate to the end of passage. By contrast, in Case D ($\theta_{inlet}^* = 0.18$ cm) and Case E ($\theta_{inlet}^* = 0.32$ cm), it is observed that CPT increases rapidly in the central portion of the passage and then tends to level off to some final value lower than that for Case F. Case C ($\theta_{inlet}^* = 0.71$ cm) agrees more with Case F except that the loss level is lower, corresponding to the lower inlet boundary layer momentum thickness. In each of the cases, the size and loss levels of the passage vortex at any given point in the passage tend to increase with inlet boundary layer momentum thickness, thus accounting for the sharp increases observed in the loss curves.

Figure 4 shows contour plots of local mass-weighted total pressure loss coefficient CPTM for selected traverse planes in Test Case D ($\theta_{inlet}^* = 0.18$ cm). These contour plots are viewed from downstream of the

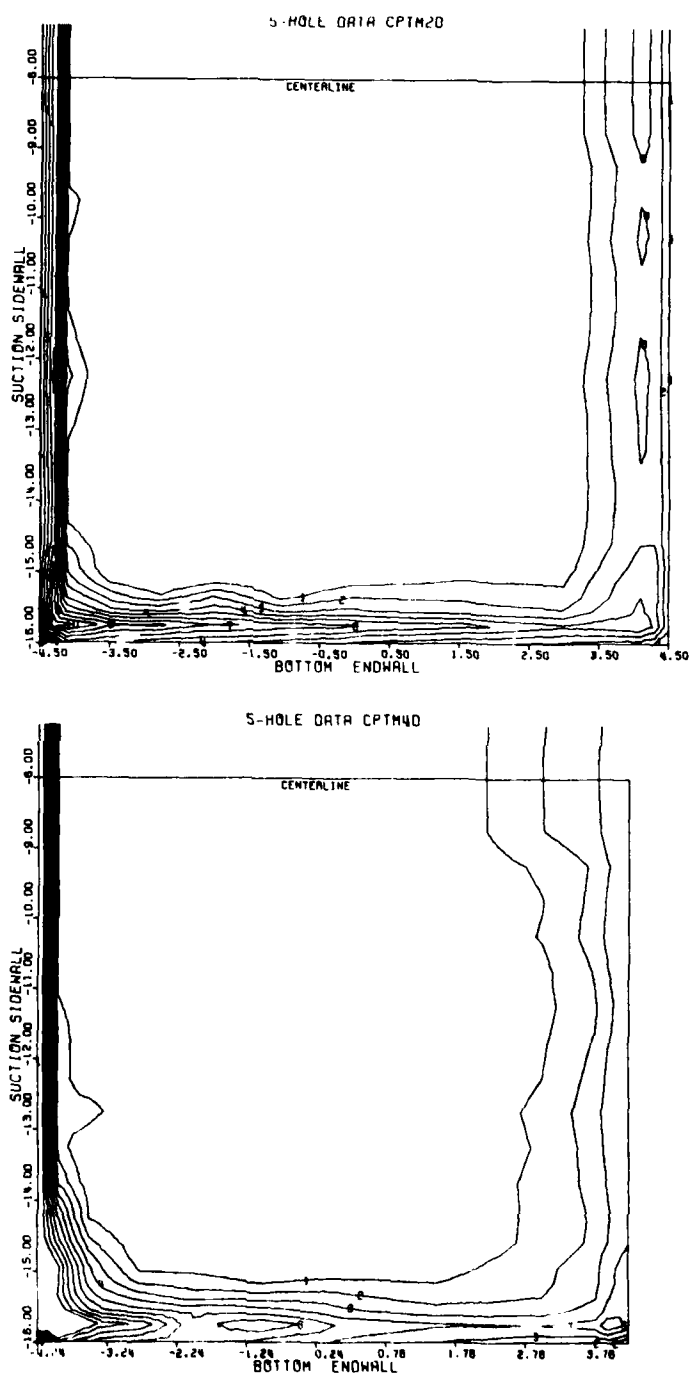


Fig. 4. Local mass-weighted total pressure loss coefficient CPTM for selected traverse planes from Test Case D.

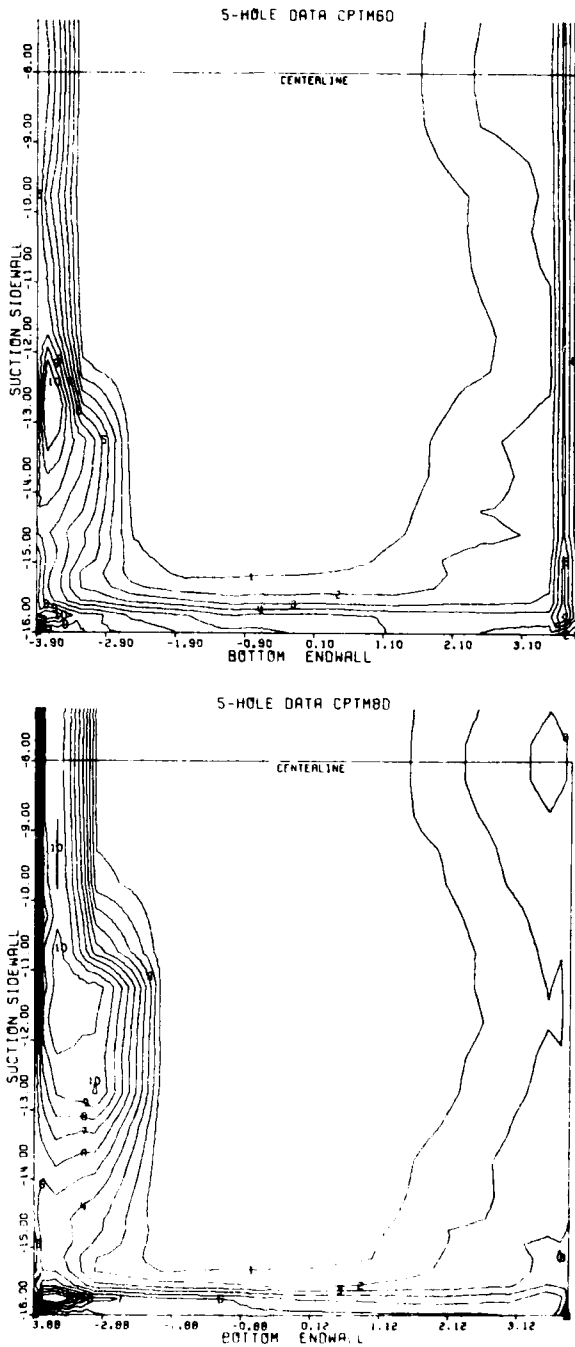


Fig. 4. (continued).

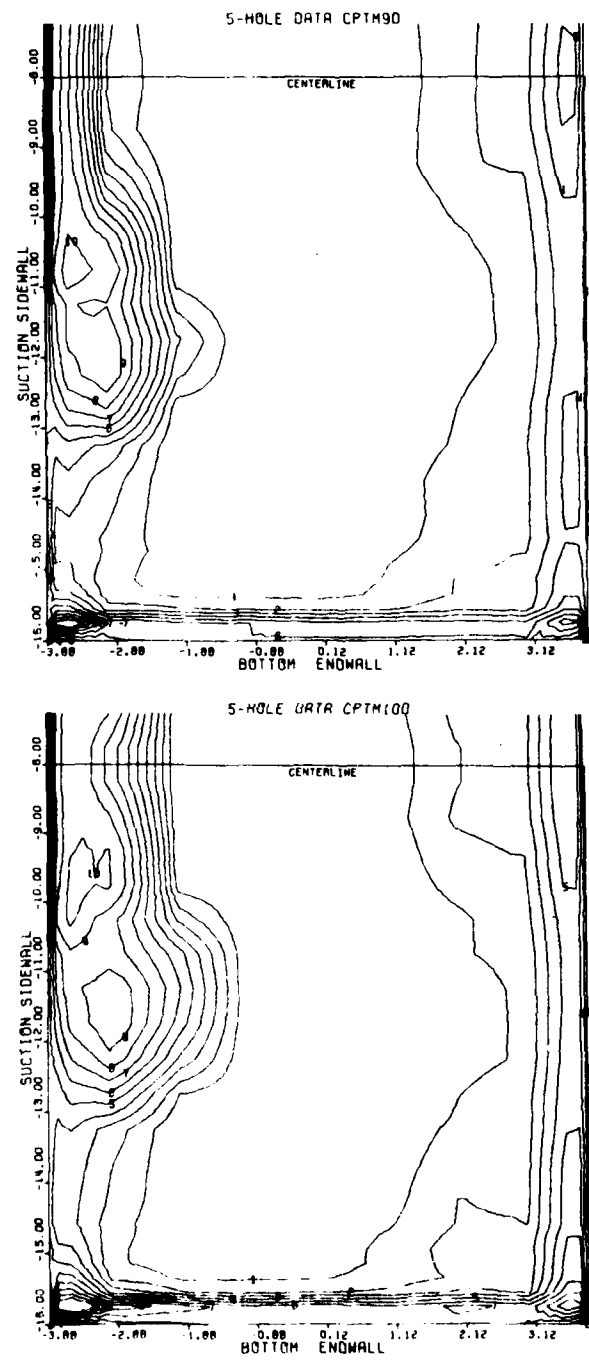


Fig. 4. (continued).

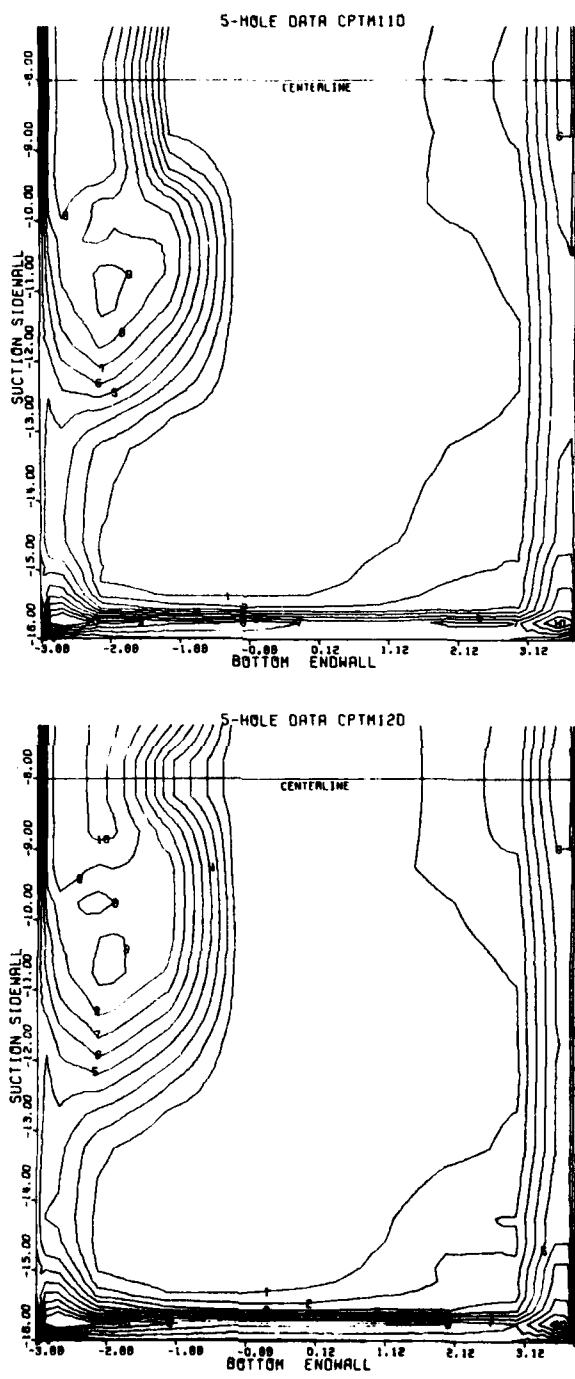


Fig. 4. (concluded).

traverse planes, with the suction sidewall (or inside of the passage bend) at the left. Because of symmetry about midspan, only the lower half of the traverse planes is shown. Higher values of the contour label number in these plots indicate higher loss levels. The contours present a consistent qualitative picture of locally mass-averaged loss behavior throughout the passage. As can be seen, in the early traverse planes (planes 2 and 4) high-loss levels are found only in the suction surface corner. This indicates that the cross flow has already swept a significant amount of low-momentum fluid into the corner to be detected. The plots for succeeding traverse planes show the further accumulation of the low-momentum fluid into the suction surface corner and its interaction with the suction surface boundary layer and their separation to form the passage vortex. As the flow progresses through the passage, the passage vortex can be seen in traverse planes 8 through 12 to grow and move up the suction sidewall towards midspan. Essentially, between traverse planes 8 and 9, the sidewall boundary layer becomes separated over the complete span. In the remaining planes, the high-loss regions of the passage vortex can be identified, as well as the growth of the vortex and its movement up the suction sidewall towards midspan. These plots indicate diffusion of the passage vortex into the main flow to mix out the total pressure losses.

Figure 5 shows contour plots of CPTM in the exit traverse plane for the four test cases. In comparing the plots, the vortex size and total pressure loss levels are seen to increase with increasing inlet boundary layer momentum thickness. Increasing order of inlet boundary layer momentum thickness occurs in Test Case D, E, C, and then F.

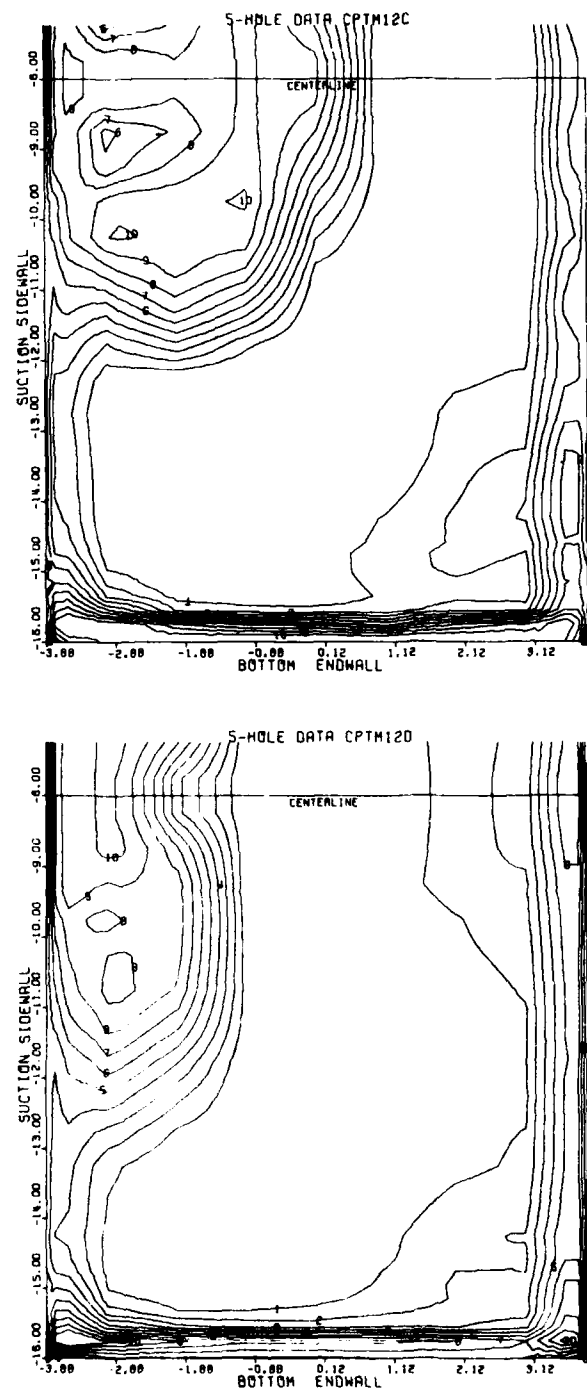


Fig. 5. Local mass-weighted total pressure loss coefficient CPTM in Traverse Plane No. 12 for the four test cases.

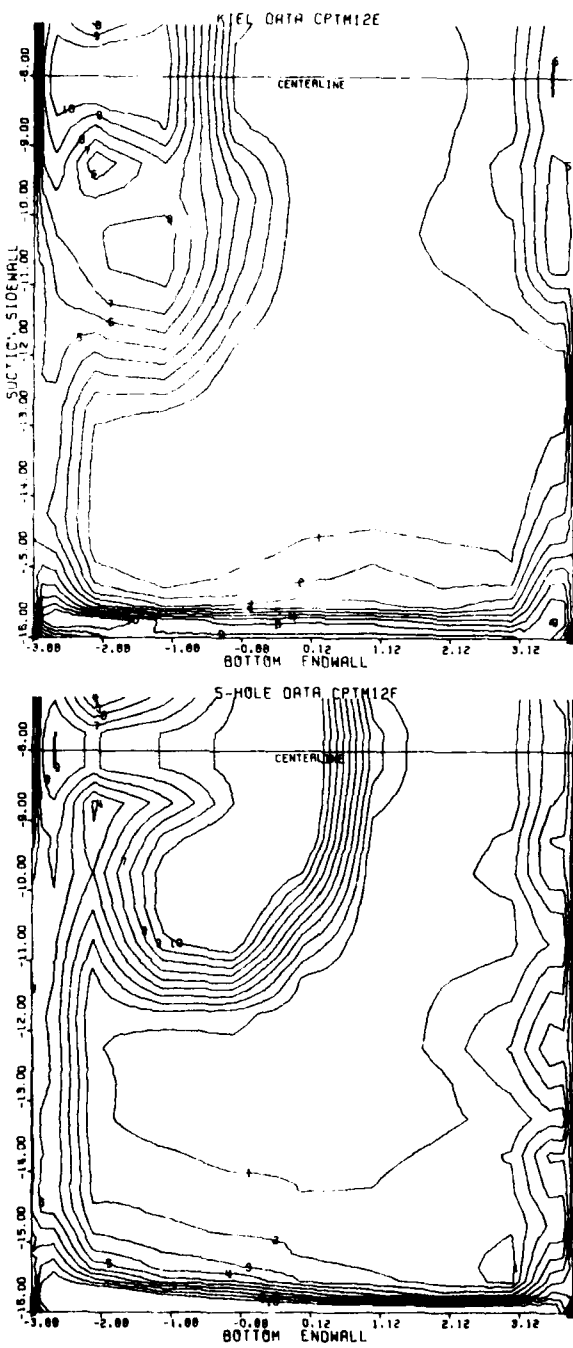


Fig. 5. (concluded).

Finally, in Figure 6, three methods of presenting total pressure loss coefficient contours are compared. The data in traverse plane 10 for Test Case C are shown. The first two plots show CPT and CPTM contours produced from probe measured points (171 points in the lower half span) and side and endwall static pressure tap measurements. Contours of CPTM in the third graph, on the other hand, were produced after enrichment of the measured data onto a uniform finely spaced grid consisting of over 2200 measured and interpolate points. In comparing these plots, greater definition of high loss regions and increased smoothness of total pressure loss coefficient contours can be observed in the enriched CPTM plot. Thus, enrichment of the data by interpolation was adopted as a standard procedure for all data reduction and contour plotting.

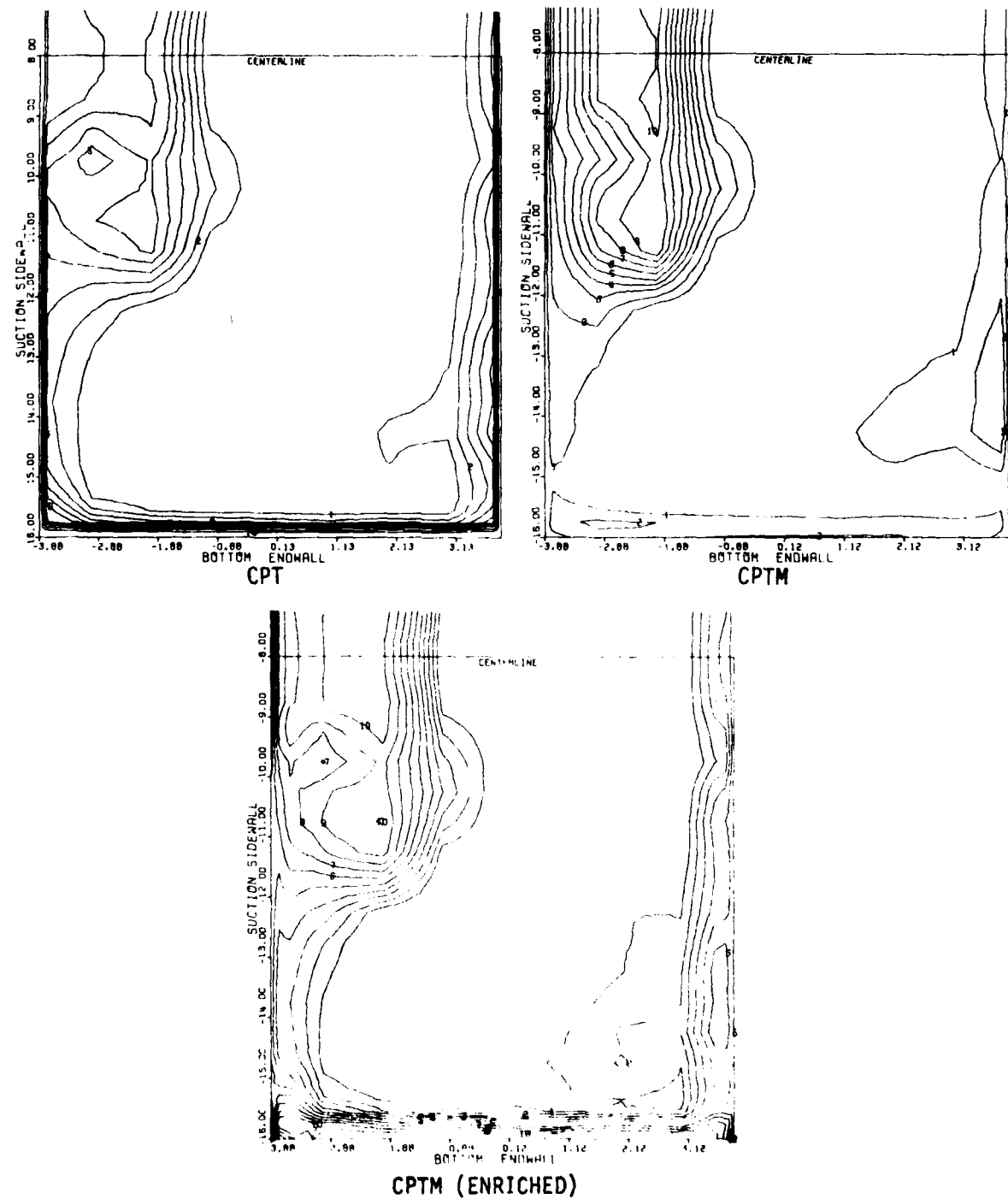


Fig. 6. Various representations of total pressure loss coefficient in Traverse Plane No. 10 for Test Case C.

2. TASK II: EXPERIMENTAL STUDY OF STATOR GEOMETRY MODIFICATIONS FOR IMPROVEMENT OF AXIAL-FLOW COMPRESSOR AERODYNAMIC PERFORMANCE

Overall performance testing of the baseline two-stage research compressor sketched in meridional plane view in Figure 7 was completed during the past year. Representative rotor and stator sections are shown in Figures 8 and 9. The related data are shown in Figure 10. The variation with flow coefficient of three important overall aerodynamic performance parameters, namely, head-rise coefficient, work coefficient, and efficiency was ascertained. The definitions of and means of evaluating each of these flow parameters and others to be discussed in this section are contained in Appendix B.

Detailed time-average aerodynamic data were also acquired in the baseline compressor at numerous axial, radial, and circumferential locations. As a representative example of blade-to-blade data currently being analyzed, some measured time-average total-head variations with circumferential extent are illustrated. Figure 11 is for flow behind the first- and second-stage rotors at several span positions, and Figure 12 is for flow behind the first- and second-stage stators at several span positions. From detailed data like these, circumferential-mean quantities have been determined which are intended to be similar to the axisymmetric-flow variables used commonly in current turbomachine design computer codes. Some sample sets of circumferential-mean data are shown in Figure 13 for flow behind the first- and second-stage rotors and in Figure 14 for flow behind the first- and second-stage stators.

During the past year, the modified stator blades (Figures 7 and 15) were fabricated out of fiberglass by Dayton Scale Model of Dayton, Ohio.

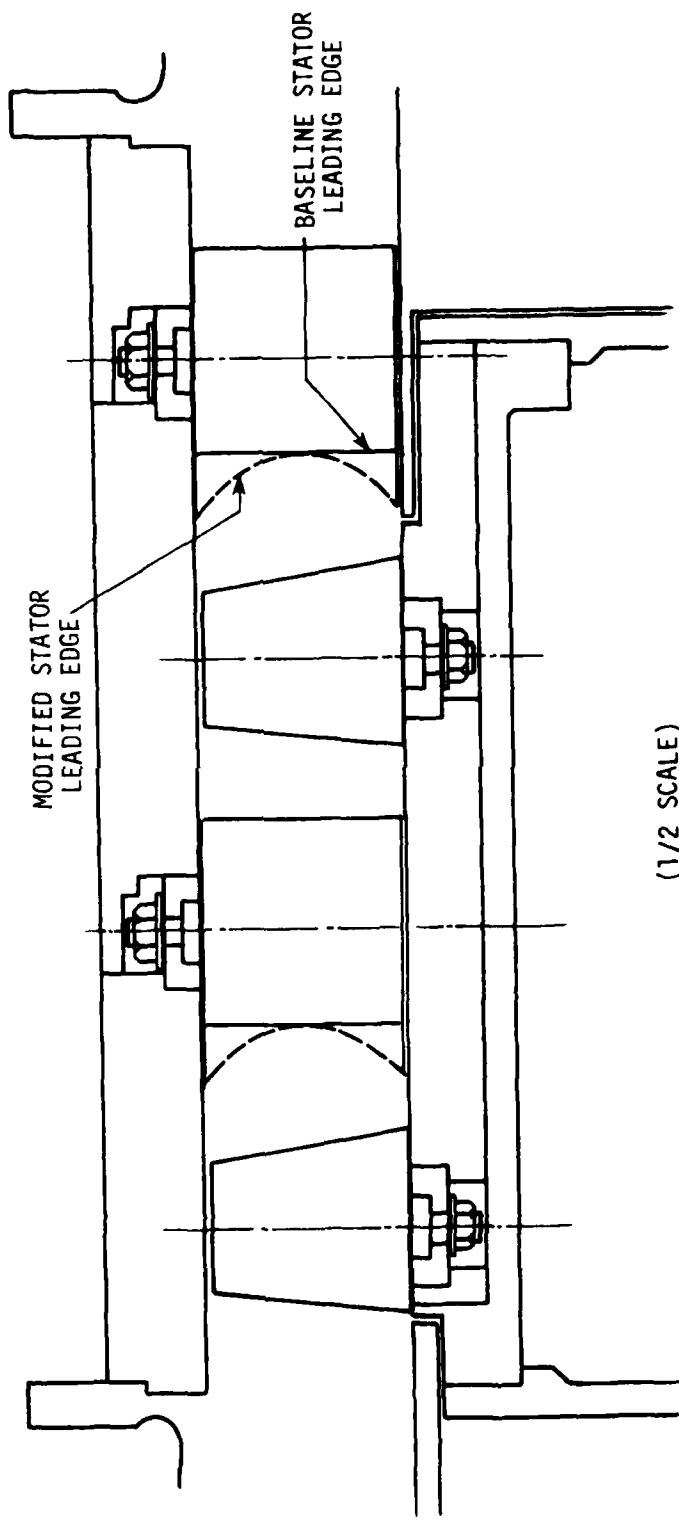


Figure 7. Meridional plane view of new blading.

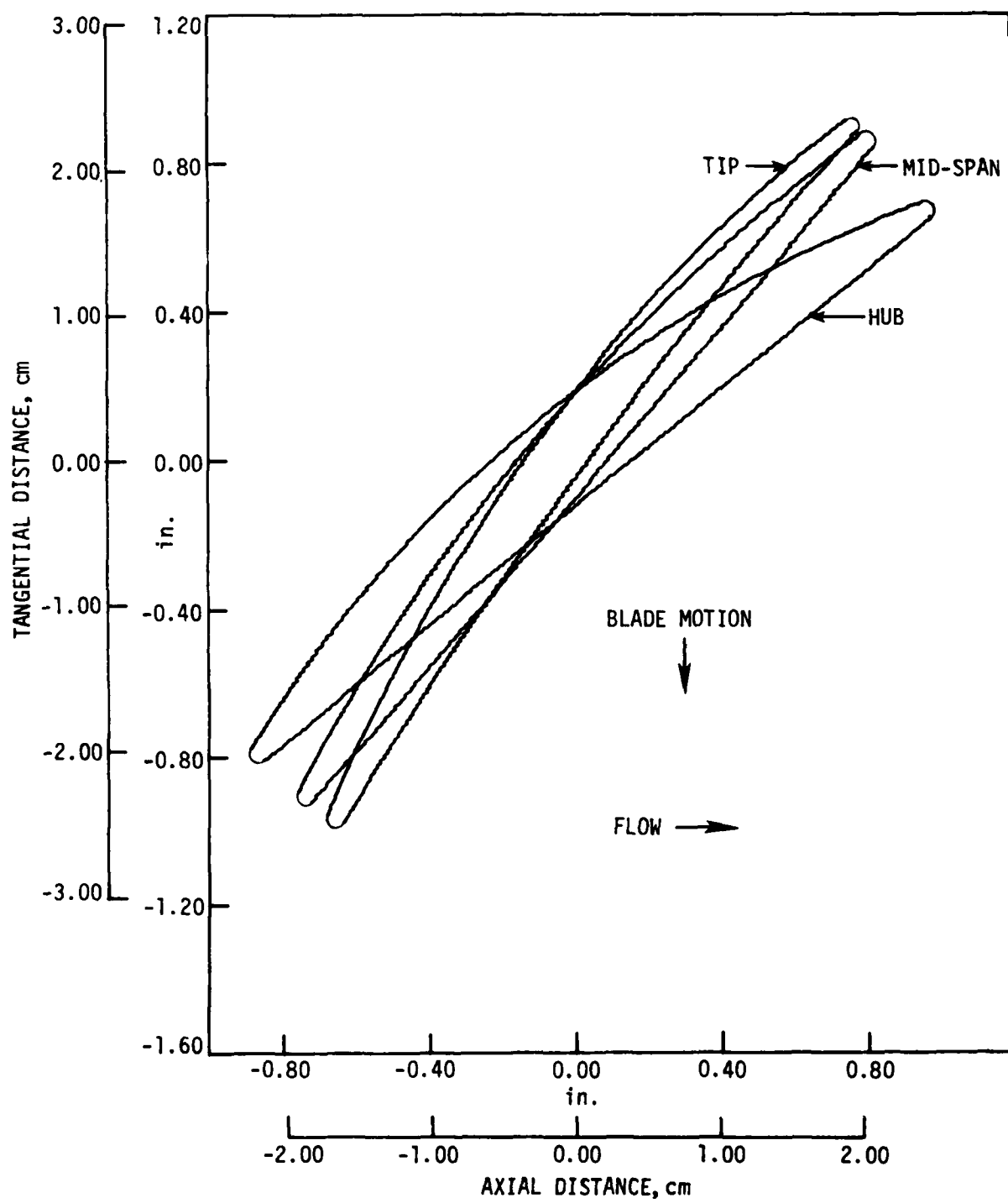


Figure 8. Representative baseline and modified compressor rotor blade sections.

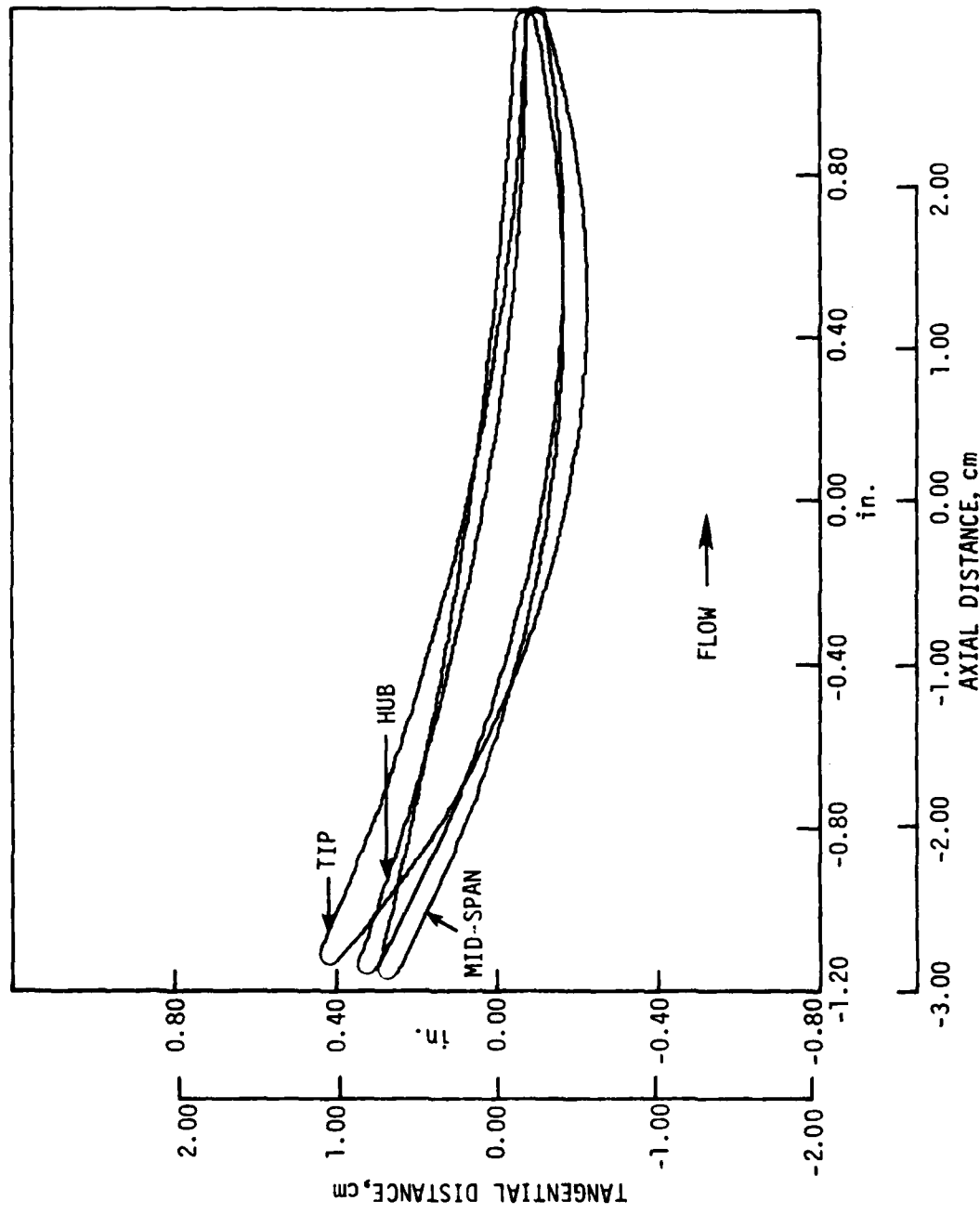


Figure 9. Representative baseline configuration stator blade sections.

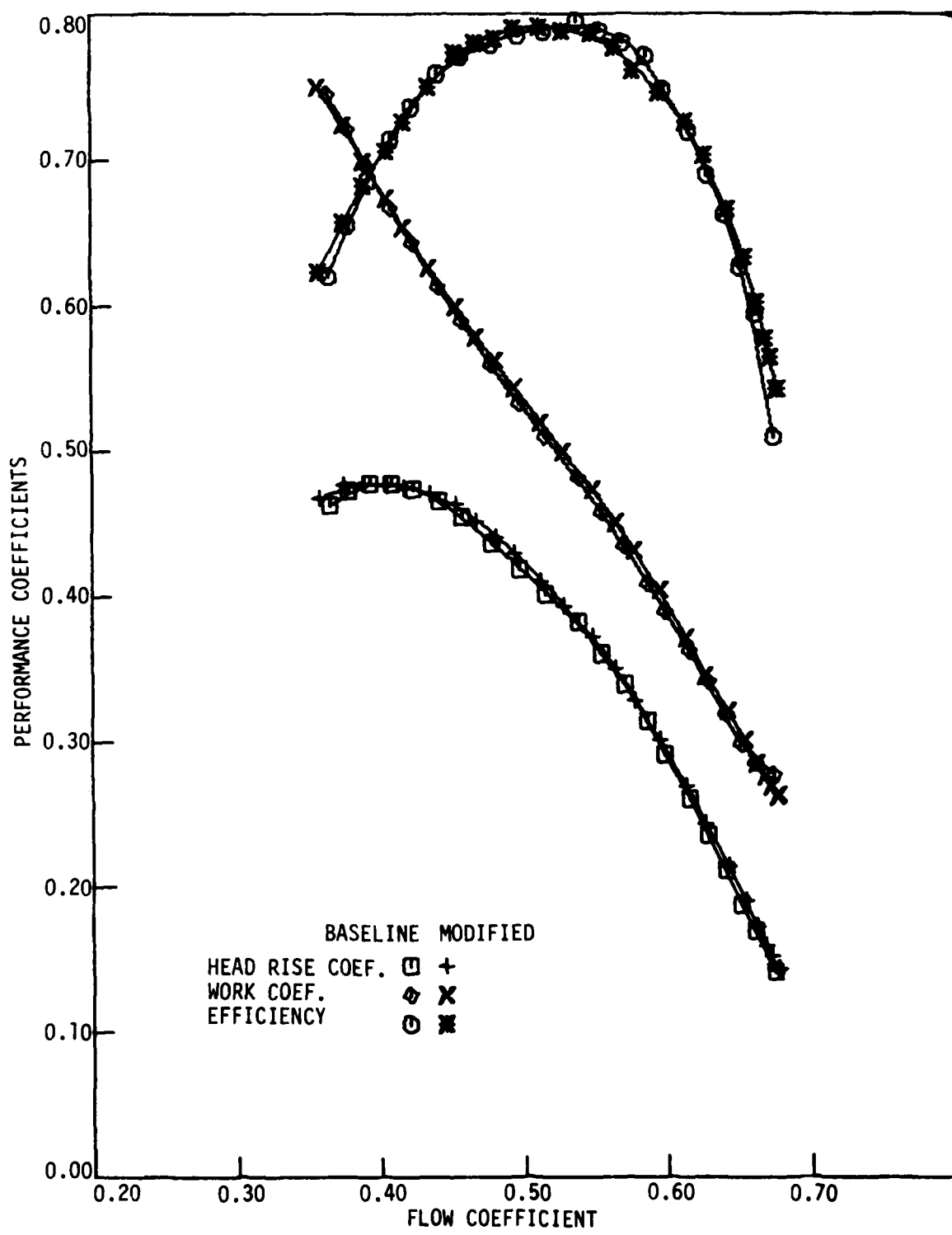


Figure 10. Overall performance data for baseline and modified compressors.

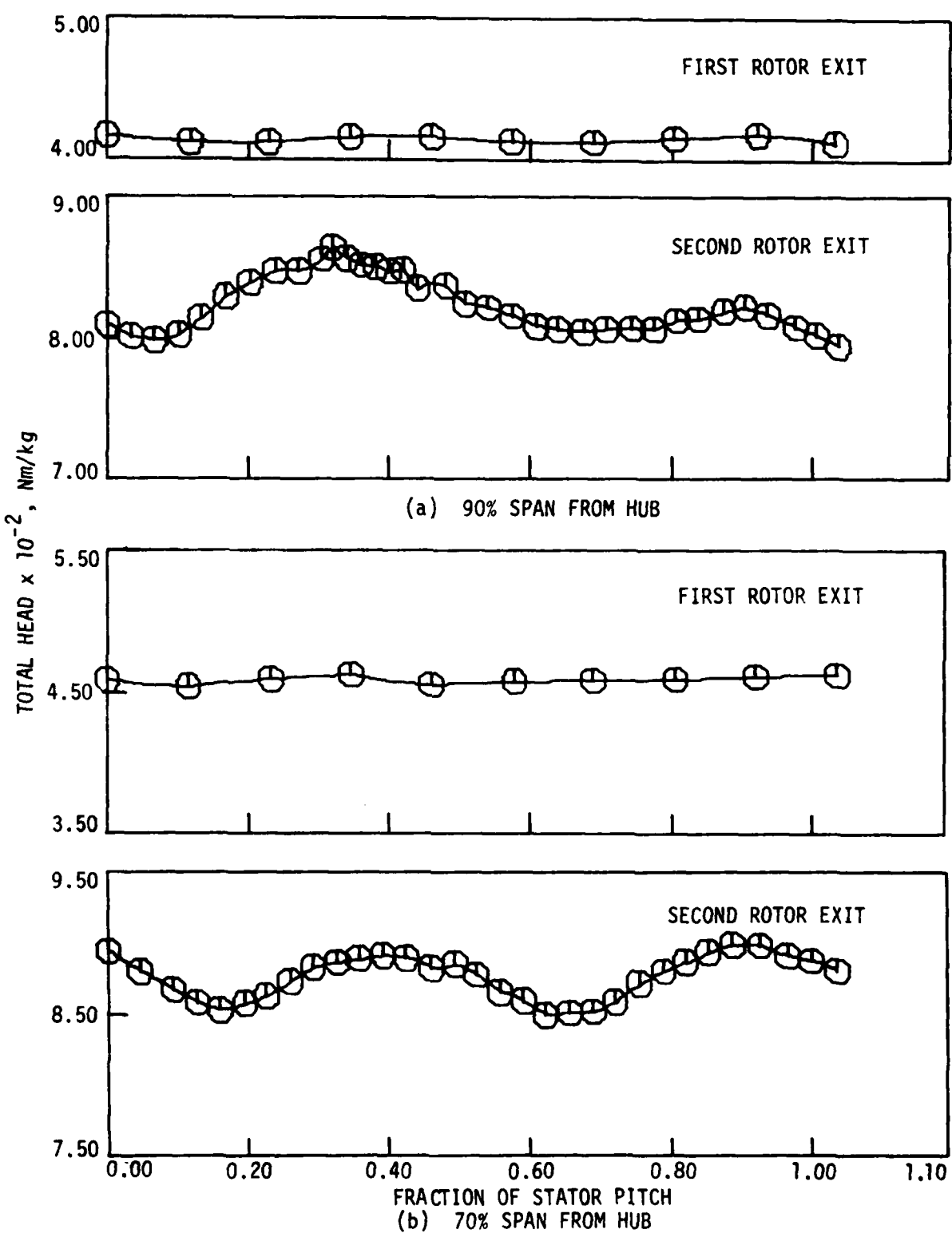


Figure 11. Blade-to-blade distribution of time-average total-head data for flow behind the first and second stage rotors of the baseline compressor for flow coefficient = 0.587.

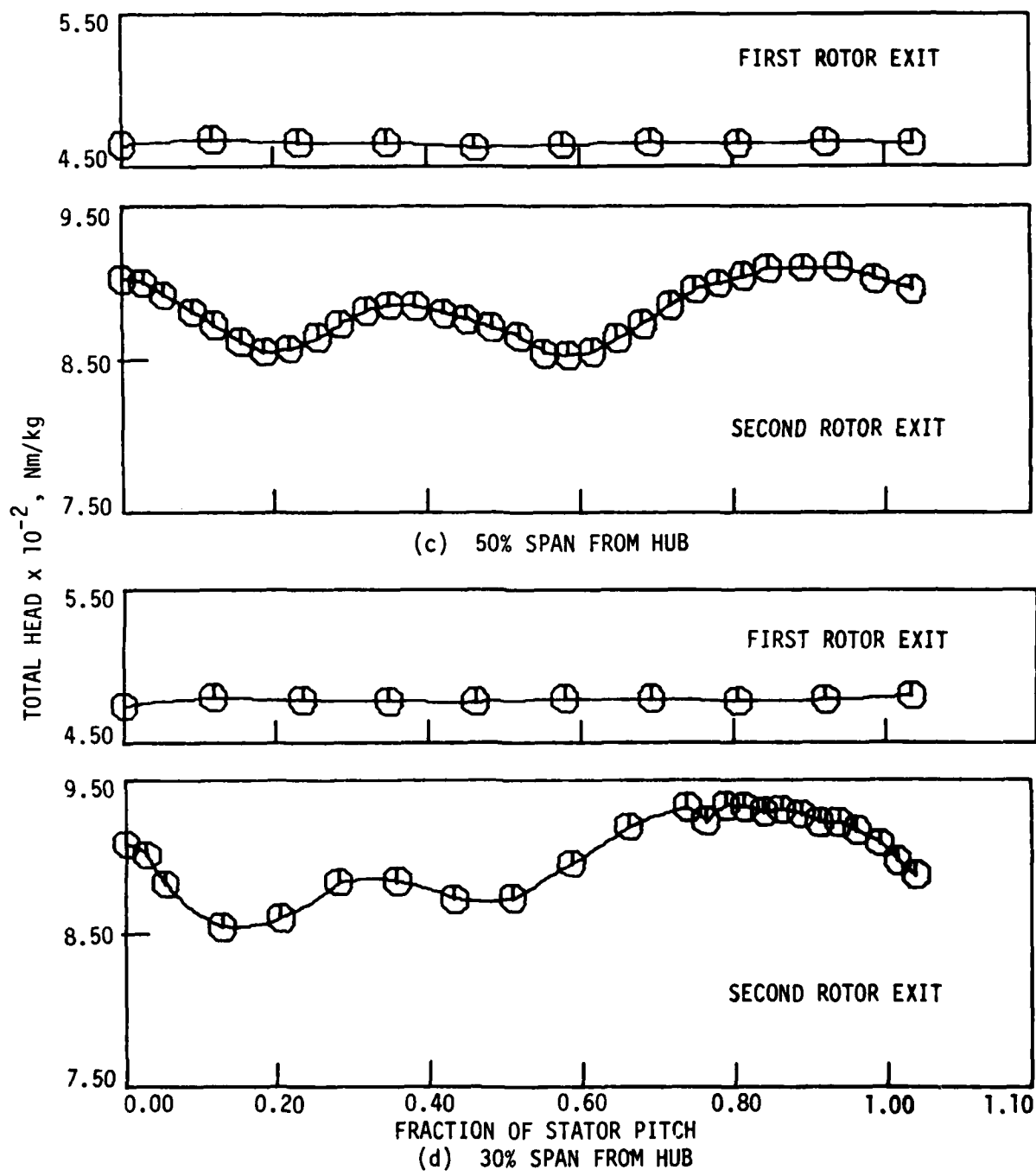


Figure 11. Continued.

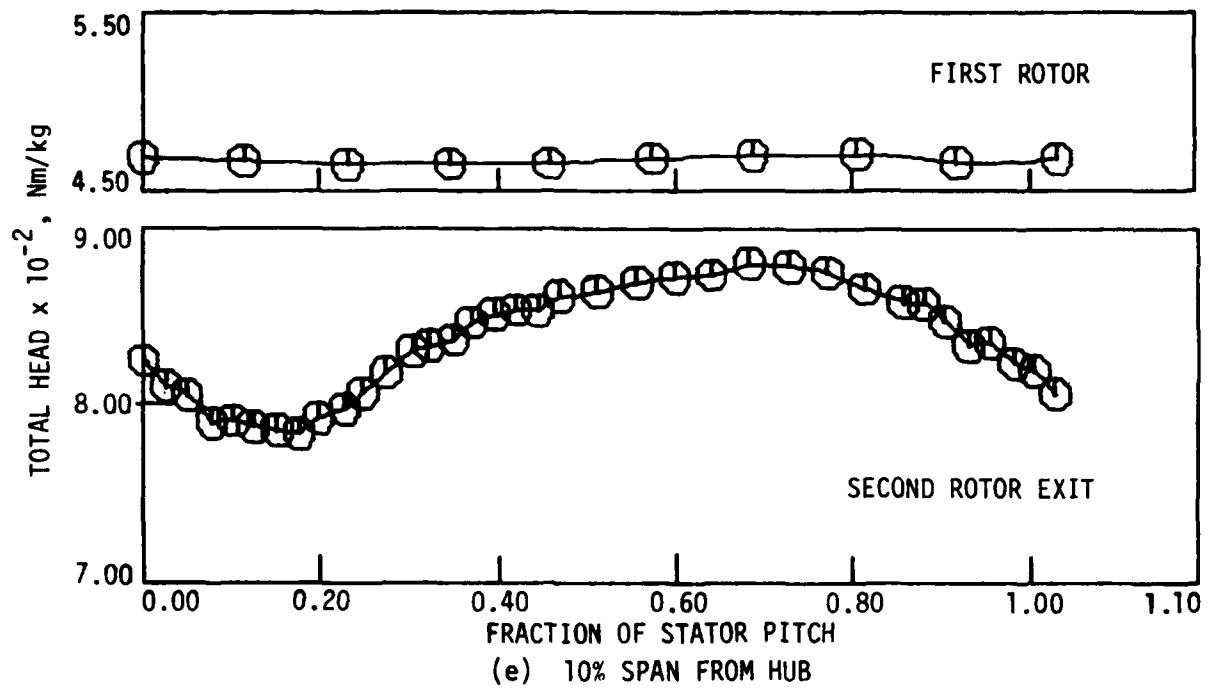


Figure 11. Concluded.

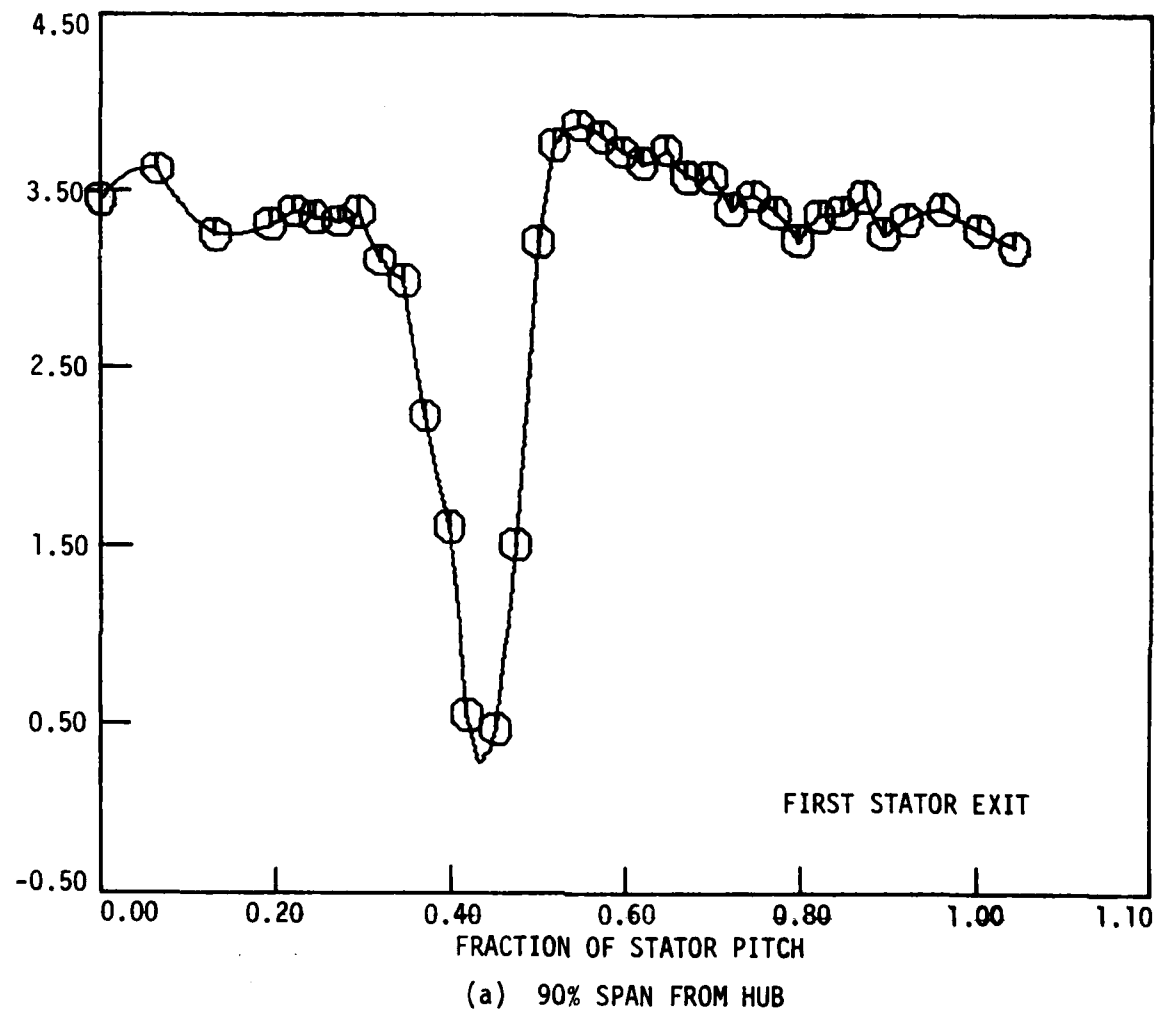


Figure 12. Blade-to-blade distribution of time-average total-head data for flow behind the first and second stage stators of the baseline compressor for flow coefficient = 0.587.

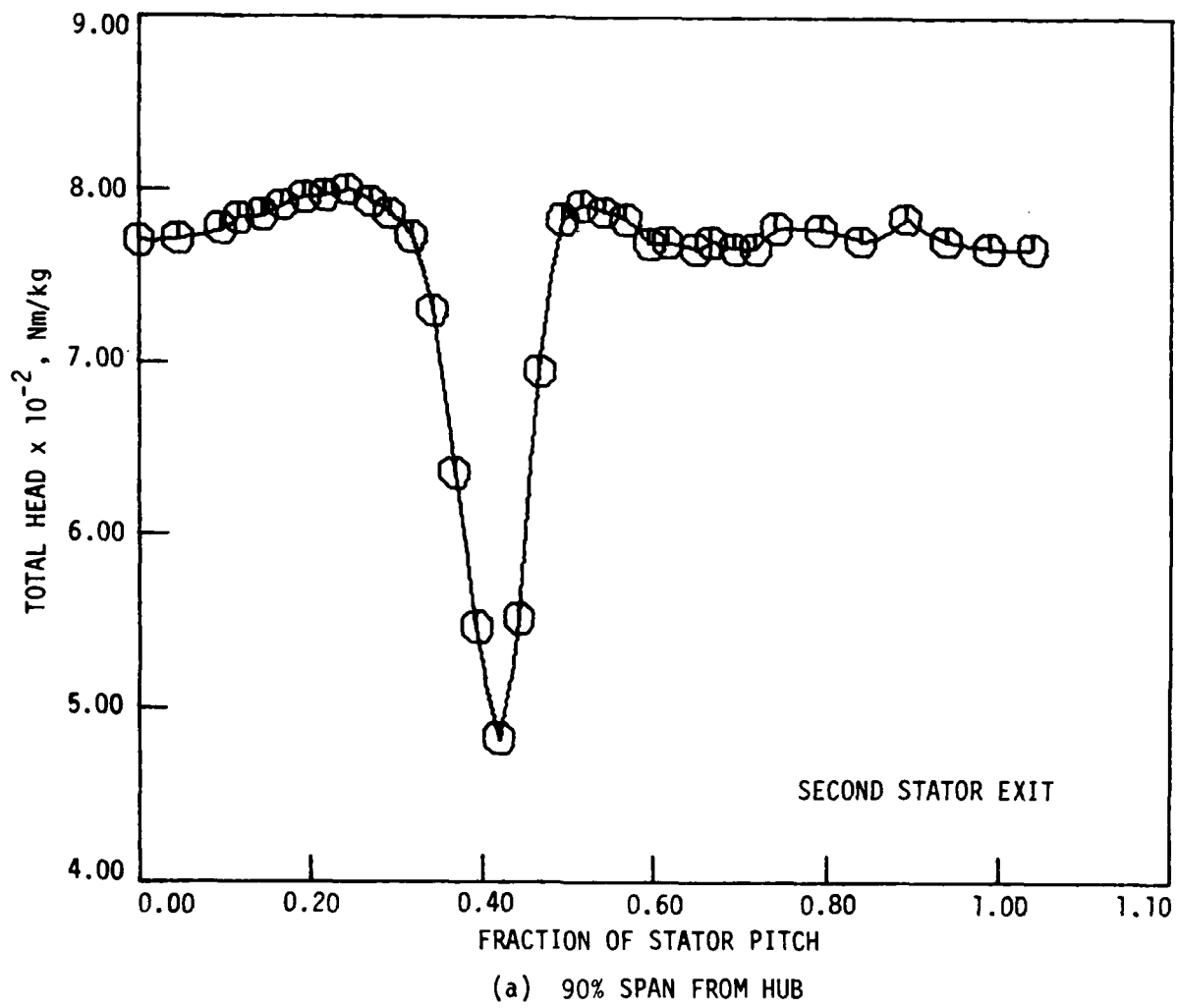


Figure 12. Continued.

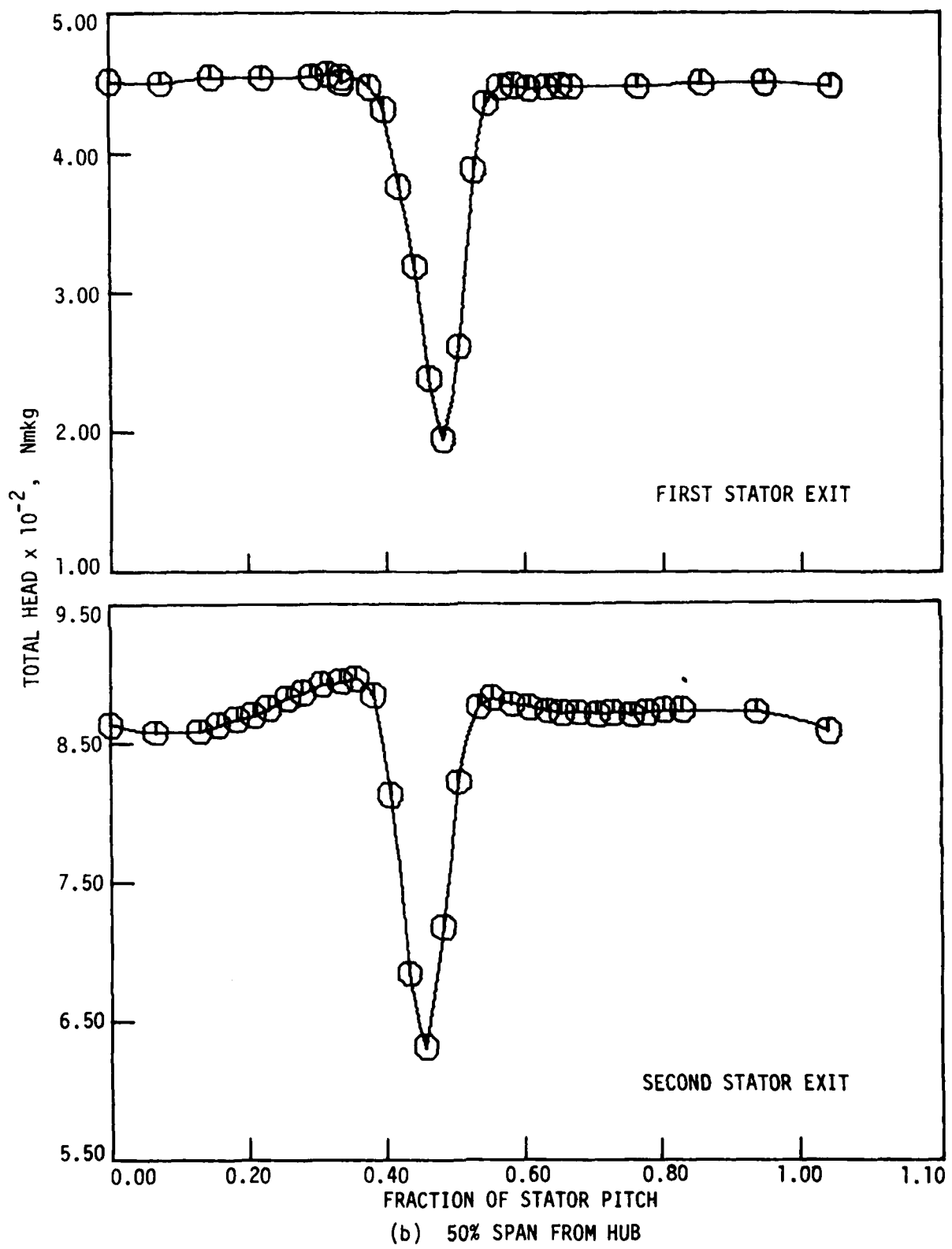


Figure 12. Continued.

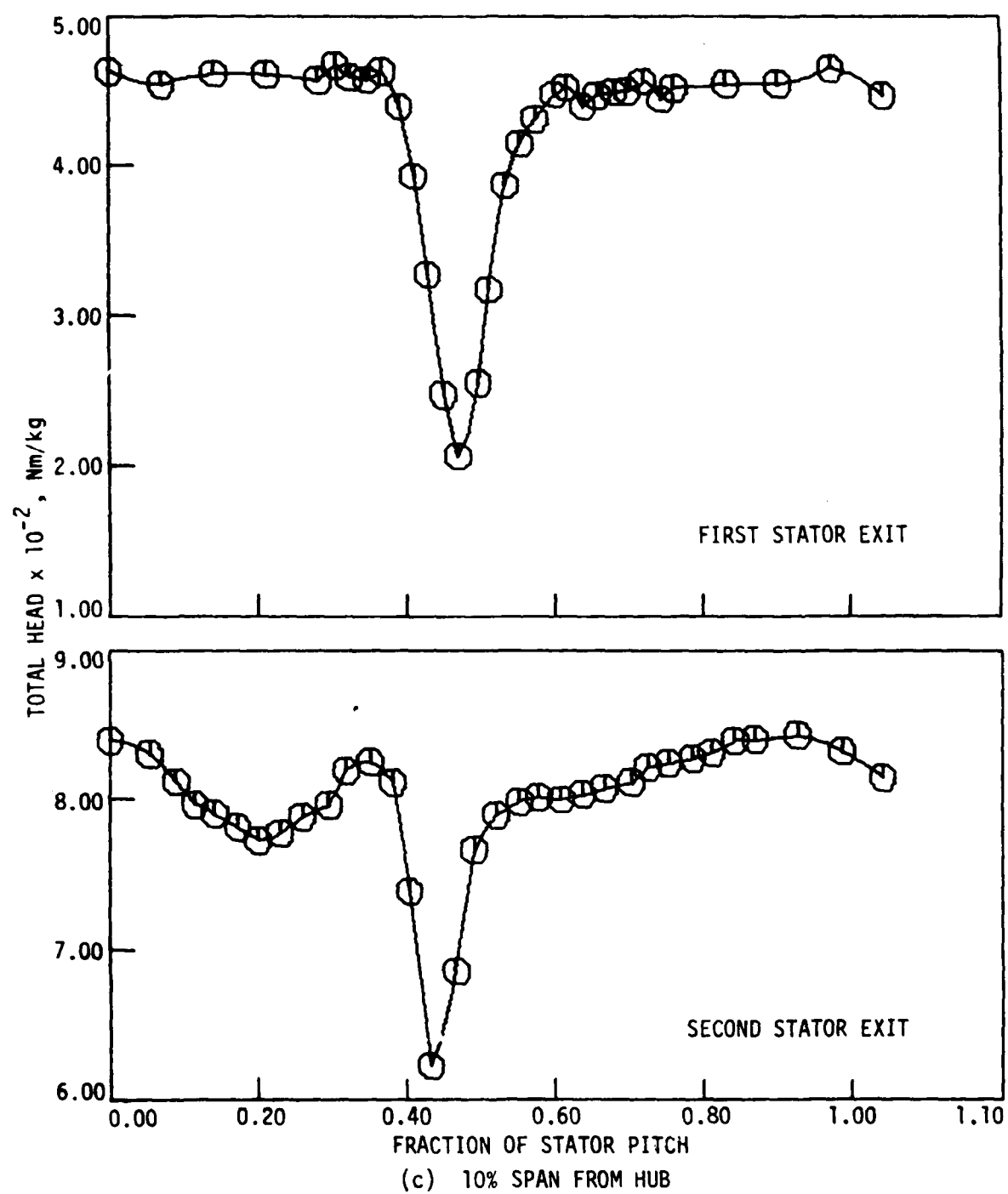
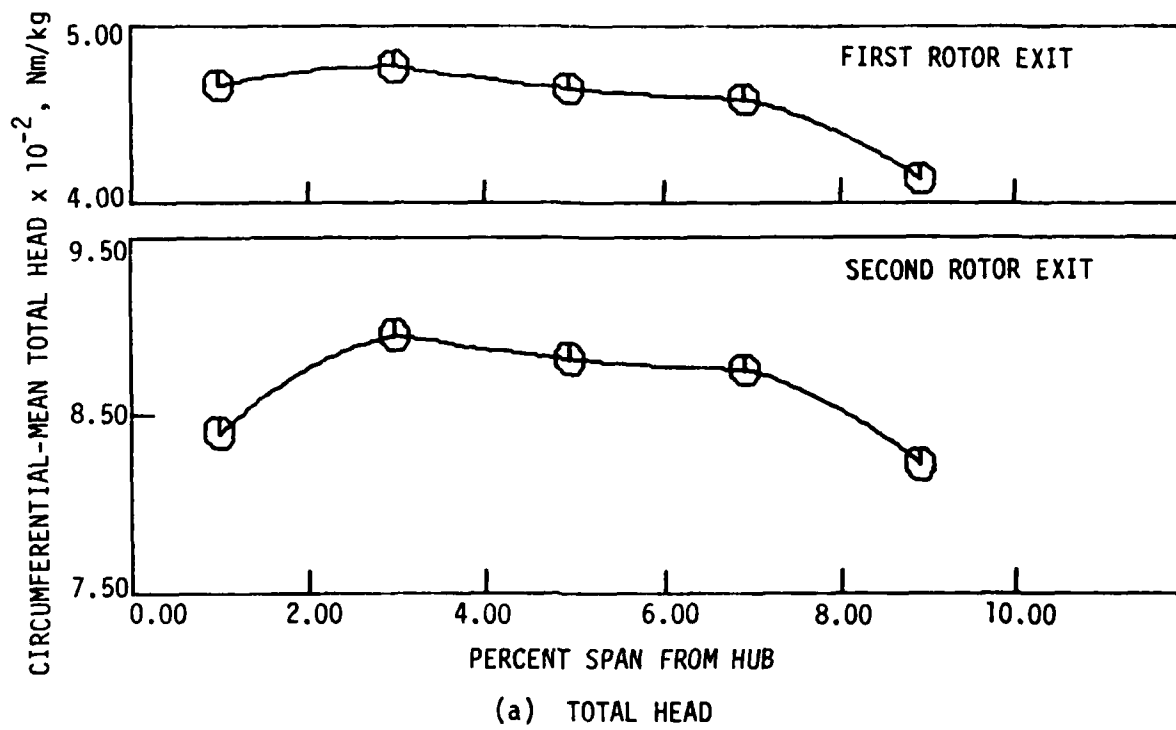


Figure 12. Concluded.



(a) TOTAL HEAD

Figure 13. Comparisons of circumferential-mean data for flow behind the first and second stage rotors of the baseline compressor for flow coefficient = 0.587.

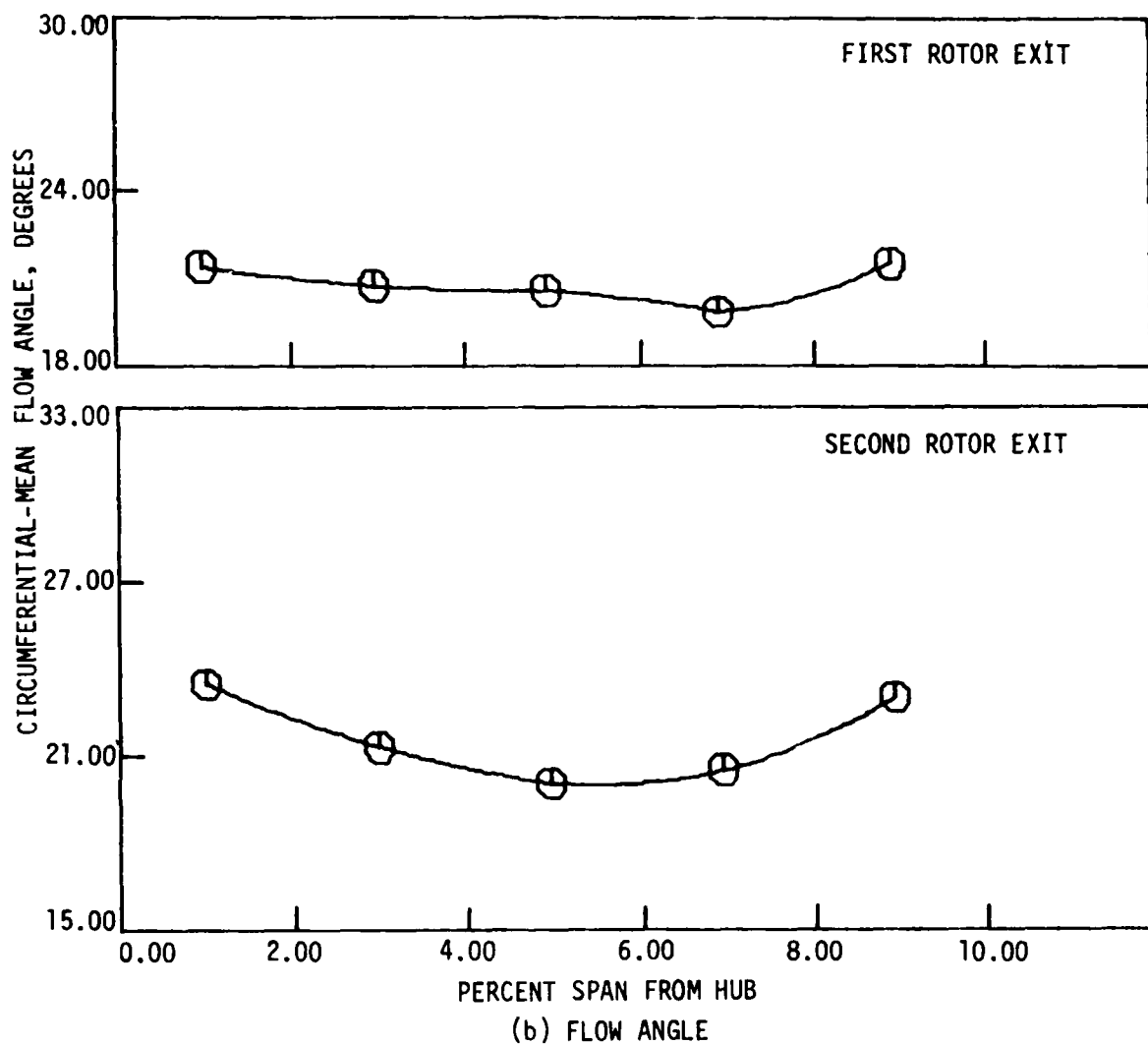


Figure 13. Continued.

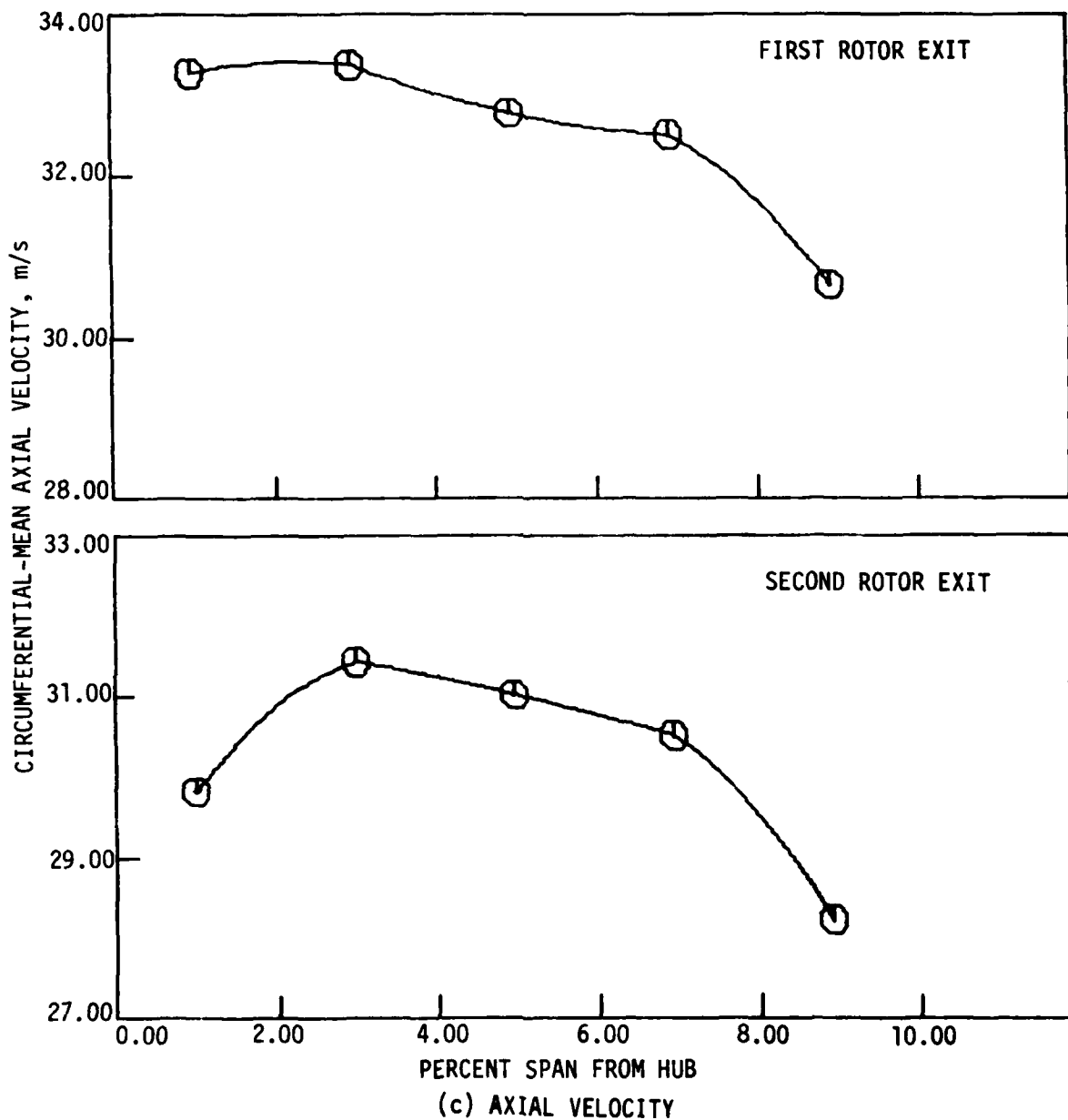


Figure 13. Concluded.

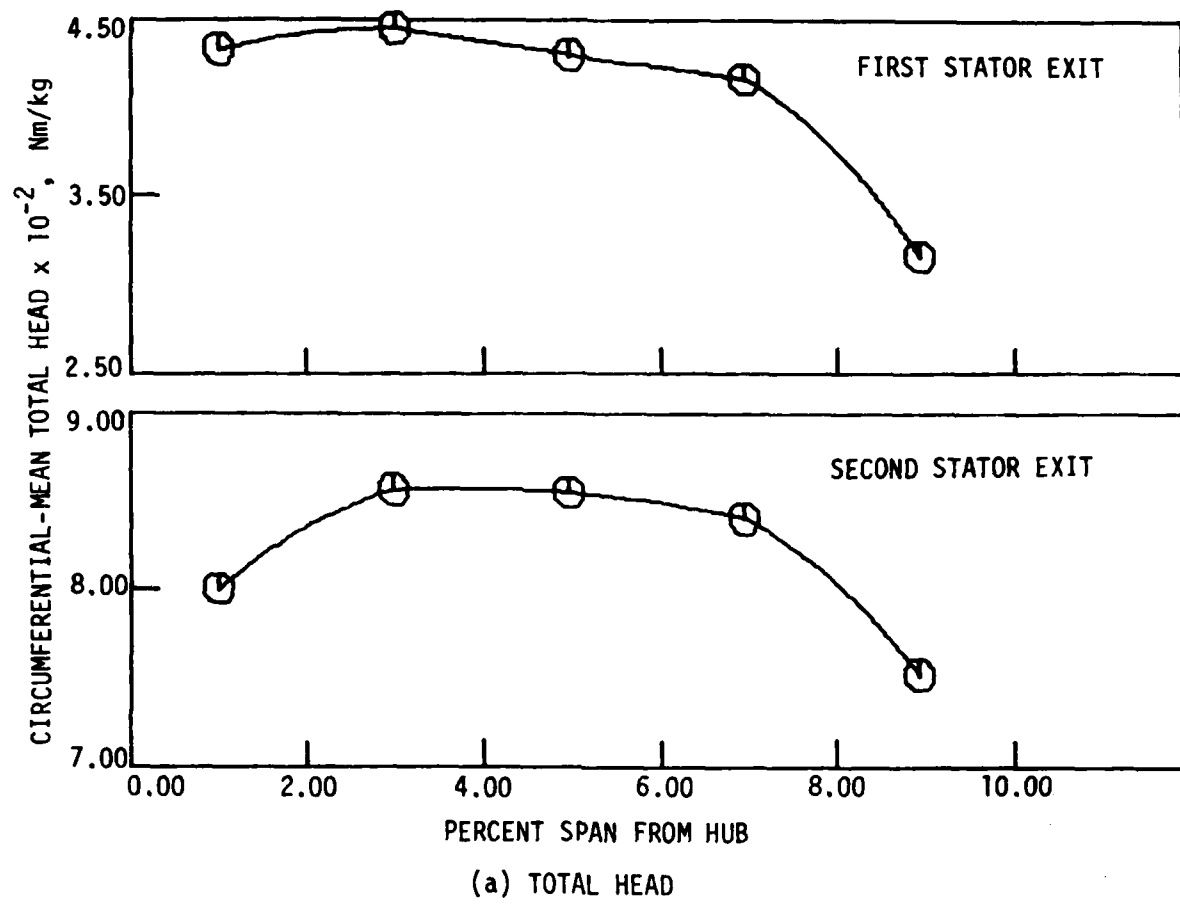
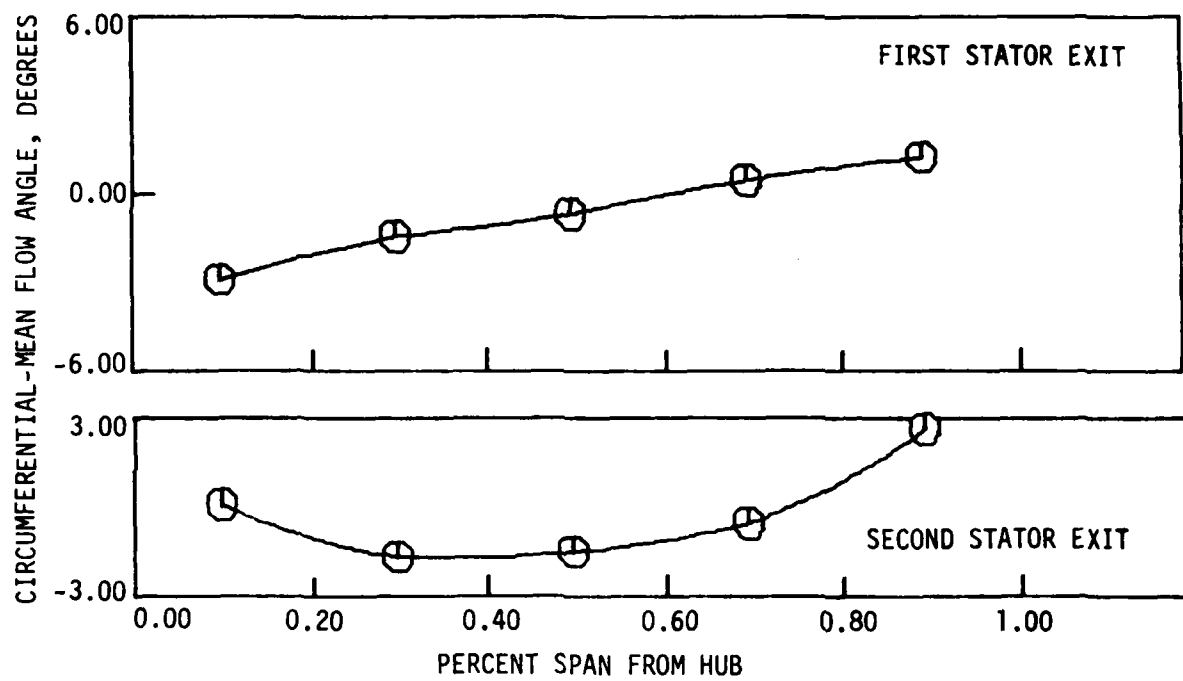


Figure 14. Comparisons of circumferential-mean data for flow behind the first and second stage stators of the baseline compressor for flow coefficient = 0.587.



(b) FLOW ANGLE

Figure 14. Continued.

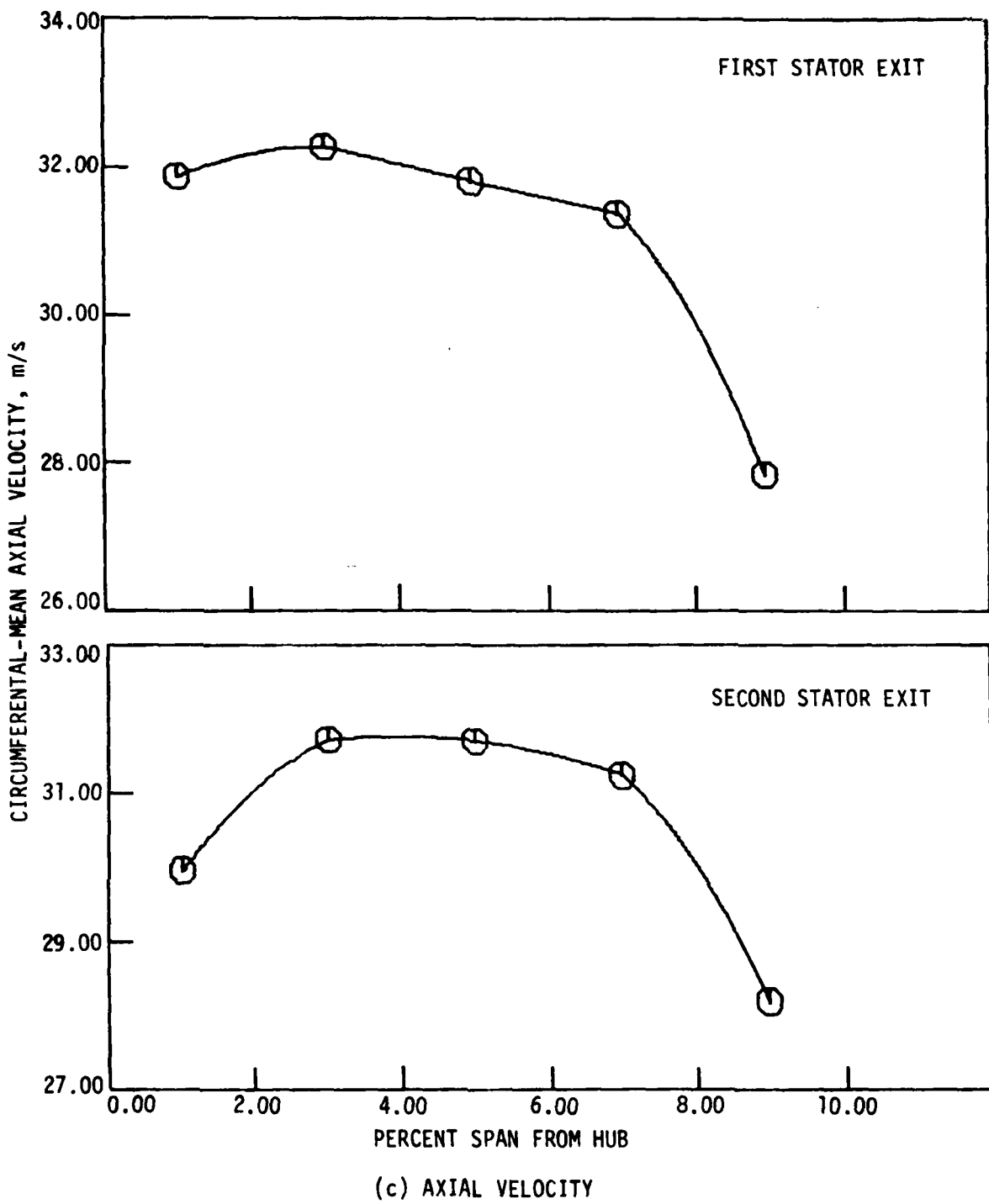


Figure 14. Concluded.

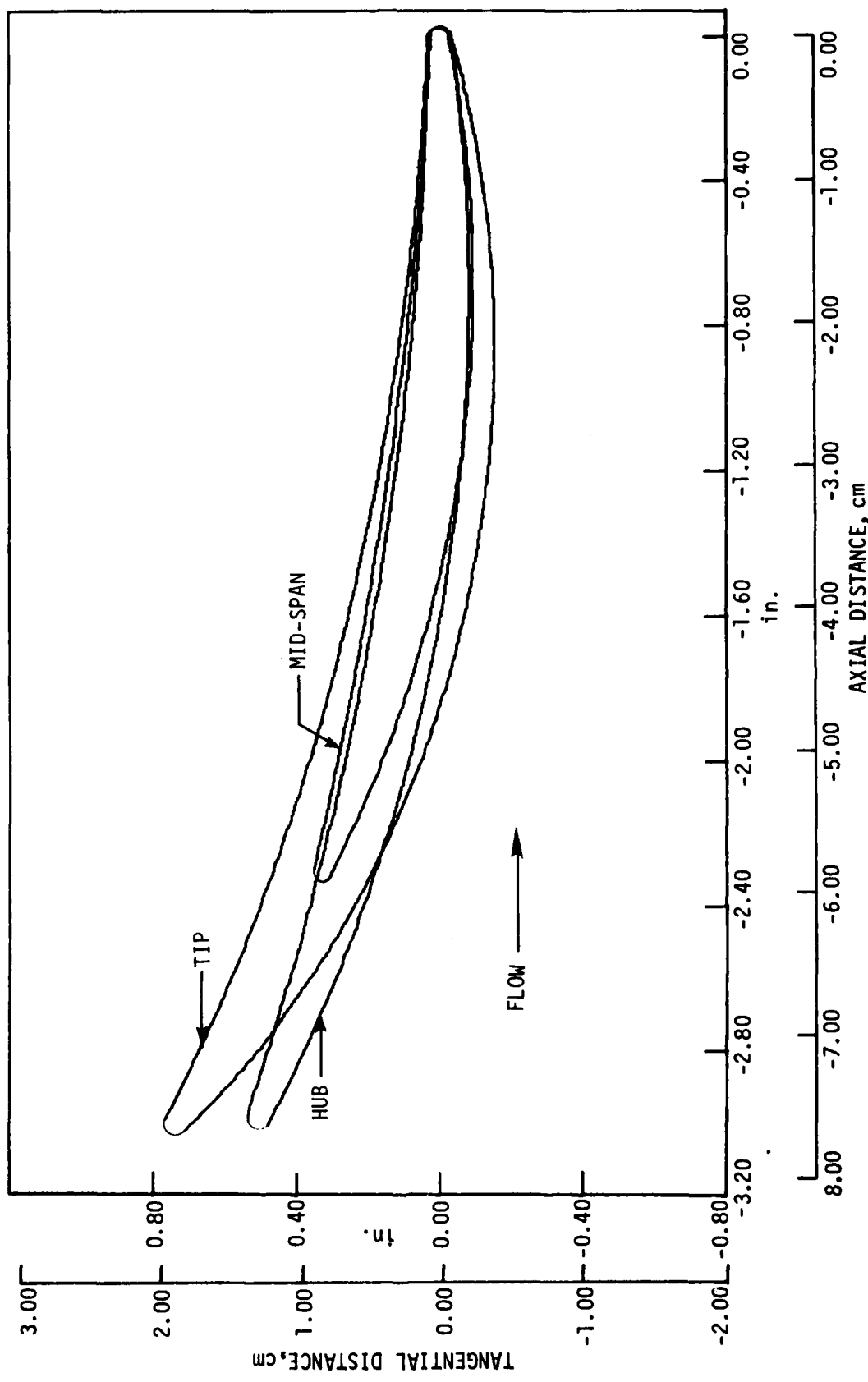


Figure 15. Representative modified stator blade sections.

These blades were subsequently set on stator rings and ground off at a constant radius to result in an appropriate cylindrical clearance (1.4% of span) above the compressor hub surface. Conventionally small corner fillets were used. In future testing, larger corner fillets will be evaluated.

Overall performance testing of the modified compressor was concluded during the past year. Results from that test are shown in Figure 10 along with the baseline compressor results. In comparing these overall performance data, one should bear in mind the similarities and differences of the two configurations as summarized below:

SIMILARITIES:

- Number of stator blades per row
- Conventional corner fillets
- Clearance between stator tip and hub surface
- Surface finish
- Mid-span chord length
- Maximum thickness to chord ratios

DIFFERENCES:

Baseline

- Stacking point at center of gravity
- No sweep/constant chord

Modified

- Stacking point at trailing edge circle center
- Symmetrical forward sweep, varying chord
- Larger solidities near hub and shroud than baseline

The precision and data repeatability associated with total head rise coefficient measurement is high enough that the slightly higher head rise achieved with the modified stator blades in portions of the flow coefficient range may be significant. This trend will be investigated further by comparing detailed data similar to those described earlier as they become available.

Efficiency data acquisition precision limitations (especially the difficulties in making good torquemeter readings) lead to an efficiency uncertainty estimate of $\pm 0.75\%$. Thus, the baseline/modified efficiency comparison is inconclusive. Stall limit data were precise enough to conclude that the modified stator blade does not offer a stall margin advantage over the baseline blade.

Testing of the baseline and modified stators will continue during the next year. In particular, more details will be acquired to make local flow comparison possible. An assessment of stator flow management gains with the modified stator will be pursued. A study of corner fillet effects on stator row flow will be initiated.

3. TASK III: AERODYNAMICS OF BLADE SURFACE BOUNDARY LAYER DEVELOPMENT IN CASCADE EXPERIMENTS AND IN COMPRESSOR OPERATION--A QUANTITATIVE EVALUATION

Task III represents the first year of work in a proposed two-year investigation. The objective of this study is to compare the numerical values of aerodynamic variables encountered in linear cascade tests and in compressor operation and to determine whether some of the performance discrepancies observed between cascade and compressor operation of similar airfoil arrays can be explained on the basis of aerodynamic variable differences. A parallel comparison is being made involving the capabilities of typical boundary-layer computation codes and the significant aerodynamic variables in cascade and compressor tests. In this case the purpose is to show whether the computation methods normally used in blade performance evaluation can reasonably be expected to produce valid results when operating within the expected aerodynamic variable ranges.

Based on the 1980-81 effort, it appears that the most obvious compressor aerodynamic variable, Mach number level, has an influence on both linear cascade and compressor airfoil turning and loss that is not adequately accounted for in performance computation using boundary layer codes. This is true in subsonic Mach number operation as well as in transonic and supersonic cases.

While a considerable amount of transonic and supersonic cascade data has been accumulated in the course of compressor component improvement programs, there has not been a great deal of work on improvement of subsonic cascade performance. In fact, in stationary blade rows of

axial-flow compressors, typical design practice leads to operation in the moderate to high subsonic Mach number range. This occurs even in those stages where rotor relative velocities are transonic and supersonic. Because stationary rows frequently contribute more than their share of losses in stage efficiency measurements, additional subsonic cascade and stator research continue to be worthwhile. Some of the current research on supercritical and controlled diffusion blade profiles has developed because of this reasoning. However, more cascade analysis and experimentation needs to be focused on the subsonic range of entrance Mach numbers, in particular to improve knowledge of the effects of Mach number on suction surface boundary layer development.

Reynolds number, turbulence intensity and scale, and surface roughness character combine to influence boundary-layer development in compressor blade configurations by affecting the location and nature of the laminar-turbulent transition region. A wide range of combinations of these variables can occur and has been observed in multistage fan and compressor operation. The envelope reported far exceeds the range of experimental values studied in linear cascade tests and the range of values ordinarily used to exercise boundary-layer computational codes.

As noted in the proposal document for Task III, there is a strong effect of axial-velocity-density product (effective stream tube area) ratio on cascade performance computation using inviscid-viscous interaction codes. While the effect is understandable, the problem remains of incorporating correct levels and distributions of the ratio into code applications. Measured distributions are slowly accumulating in current experimental programs. It is difficult to predict the extent to which

the data will be made available, and the quality of the data should be subject to study before it is used in the current work.

Another variable totally unaccounted for in linear cascade testing or computation is the unsteadiness present in compressor flows due to upstream row wakes and wake chopping. This is a complex matter, not well understood and lacking in even simple parametric analysis. Such an analysis has been in progress during the last few months of the 1980-81 Task III program.

It is interesting to note that while the significance of the aerodynamic variables under consideration has been repeatedly and strongly reported in papers and texts in fundamental fluid dynamics over a long period, the recognition of this significance in turbomachinery analysis has not been satisfactory. These variables are not of secondary importance in compressor and turbine flows. Therefore, Task III and similar research studies should continue to receive attention.

References 3 through 8 are selected reports contributing to the work of Task III.

SECTION III. PUBLICATIONS

The following list includes documents published since October 1, 1980 that are based entirely or in part on research supported by the AFOSR.

1. Hansen, E. C., Serovy, G. K., and Sockol, P. M. Axial-Flow Compressor Turning Angle and Loss by Inviscid-Viscous Interaction Blade-to-Blade Computation. *Journal of Engineering for Power, Trans. ASME.* 102: 28-34, 1980.
2. Hansen, E. C., Serovy, G. K., and Sockol, P. M. Axial-Flow Compressor Turning Angle and Loss by Inviscid-Viscous Interaction Blade-to-Blade Computation. *NASA Technical Note (In preparation).*
3. Hottman, D. A. Turbomachinery Laboratory Data Acquisition and Experiment Control Systems. *Iowa State University Engineering Research Institute Technical Report TCRL-19,* 1980.
4. Kluck, C. E. Prediction of Laminar-to-Turbulent Boundary Layer Transition in Axial-Flow Turbomachinery. *Turbomachinery Components Research Program, Iowa State University, TCRL-21,* September 1981.
5. Okiishi, T. H. Periodically Unsteady Flow Through an Imbedded Stage of a Multistage Axial-Flow Turbomachine. In Aeroelasticity of Turbine Engines, Joint NASA/AF/Navy Symposium Preprint, October 1980.
6. Serovy, G. K., and Hansen, E. C. Computation of Flow in Radial- and Mixed-Flow Cascades by an Inviscid-Viscous Interaction Method. In Centrifugal Compressors, Flow Phenomena and Performance, AGARD-CP-282, 1980.

7. Serovy, G. K. Deviation/Turning Angle Correlations. Final Report of AGARD/PEP Working Group 12 on Through-Flow Calculations in Turbomachines (In publication).
8. Serovy, G. K. Axial-Flow Turbomachine Through-Flow Calculation Methods. Final Report of AGARD/PEP Working Group 12 on Through-Flow Calculations in Turbomachines (In publication).
9. Smith, P. Flow Calibration of Five-Hole Directional Pressure Probes. Iowa State University Engineering Research Institute Technical Report TCRL-20 (In publication).
10. Zierke, W. C., and Okiishi, T. H. Measurement and Analysis of the Periodic Variation of Total Pressure in an Axial-Flow Compressor Stage. Iowa State University Engineering Research Institute Technical Report TCRL-18, November 1980.
11. Zierke, W. C., and Okiishi, T. H. Measurement and Analysis of Total-Pressure Unsteadiness Data from an Axial-Flow Compressor Stage. ASME Paper No. 81-Gr/GT-2, Presented at the International Symposium on Applications of Fluid Mechanics and Heat Transfer to Energy and Environmental Problems, University of Patras, Patras, Greece, June 29-July 3, 1981.

SECTION IV. PROGRAM PERSONNEL

Three principal investigators share responsibility for the current program.

- George K. Serovy, Anson Marston Distinguished Professor in Engineering, Tasks II and III
- Patrick Kavanagh, Professor of Mechanical Engineering, Task I
- Theodore H. Okiishi, Professor of Mechanical Engineering, Task II

Six graduate-level engineers have also been associated with the work.

- John A. McAndrew, Graduate Research Assistant, Task I
- C-H. Shyh, Graduate Research Assistant, Task I
- Michael D. Hathaway, Graduate Research Assistant, Task II
- Daniel L. Tweedt, Graduate Research Assistant, Task II
- William C. Zierke, Graduate Research Assistant, Task II
- Ruth A. Spear, Graduate Research Assistant, Task III

During the research several undergraduate students in Mechanical Engineering have made useful contributions. This is an effective mechanism for introducing undergraduates to the research activity in turbomachinery.

- Keith A. Dau-Schmidt, Undergraduate Assistant, Task I
- Mark T. Diefenthaler, Undergraduate Assistant (to 1 March 1981), Task I
- Douglas A. Hottman, Undergraduate Assistant (to 1 December 1980), Task I
- Gregory R. Palczewski, Undergraduate Assistant, Task I

- Paul G. Smith, Undergraduate Assistant (to 1 March 1981), Task I
- Robert A. Uhlig, Undergraduate Assistant, Task I
- Gary P. Campbell, Undergraduate Assistant, Task II

SECTION V. INTERACTION WITH UNITED STATES AND FOREIGN GOVERNMENT
AGENCIES AND INDUSTRY

The turbomachinery research program at Iowa State University has focused on projects which make a contribution to the development of design systems for advanced compressors, fans, and turbines for air-breathing aircraft propulsion systems. The current grant has not changed this focus and has involved numerous direct contacts with outside organizations.

Task II depends on substantial cooperation with USAF/AFAPL and industry. A list of the visits and telephone contacts for Task II follows.

<u>Organization and Nature of Contact</u>	<u>Individual Contacts</u>
NASA-Lewis Research Center, Cleveland, Ohio; lab visits and technical dis- ussions	C. Ball J. E. Crouse D. M. Sandercock Dr. A. J. Strazisar
Air Force Aero Propulsion Laboratory, Wright-Patterson Air Force Base, Ohio; technical discussions	Dr. A. J. Wennerstrom
General Electric Company, Advanced Turbo- machinery Aerodynamics, Cincinnati, Ohio; discussion of blade fabrication problems	Dr. D. C. Wisler

<u>Organization and Nature of Contact</u>	<u>Individual Contacts</u>
Pratt & Whitney, East Hartford, Connecticut; discussion of blade fabrication problems	H. Weingold
Air Research, Phoenix Division, Phoenix, Arizona; tests cases	J. R. Switzer P. Dodge
Institut für Antriebstechnik, Deutsche Forschungs- und Versuchsanstalt für Luft- und Raumfahrt, Köln, West Germany; test cases, review of results	Dr. G. Winterfeld Dr. H. Starken Dr. H. B. Weyer
Direction de l'Energetique, Office National d'Etudes et de Recherches Aérospatiales, Châtillon-sous-Bagneux, France; test cases, review of results	J. Fabri G. Meauzé P. Bry
NASA-Lewis Research Center, Cleveland, Ohio; computation, test cases, review of results	D. M. Sandercock T. Gelder

SECTION VI. DISCOVERIES, INVENTIONS,
AND SCIENTIFIC APPLICATIONS

No fundamentally new concepts or devices were developed. However, Task II involves some blade design concepts which originated in AFAPL and may, after experimental evaluation and development, lead to improved multi-stage compressor performance.

SECTION VII. CONCLUDING REMARKS

The one-year period covered by AFOSR Grant 81-0004 was characterized by the accumulation and analysis of experimental data in Tasks I and II and by the collection of outside data to support the analysis of Task III. The technical achievements have been summarized in this report.

There is a second element in university research that is probably of greater long-term significance than the research data obtained. The overall research program on Aerodynamics of Advanced Axial-Flow Turbomachinery, now completing its third year, has produced a coordinated effort involving faculty, graduate students, and undergraduate assistants. The resulting continuity allows the development of people as well as useful research information.

REFERENCES

1. Serovy, G. K., P. Kavanagh, and T. H. Okiishi. Aerodynamics of Advanced Axial-Flow Turbomachinery. Final Report, 1 October 1978 - 30 September 1980. Technical Report TCRL-17, Turbomachinery Components Research Program, Department of Mechanical Engineering and Engineering Research Institute, Iowa State University, Ames, Iowa, 1980.
2. Hottman, D. A. Turbomachinery Laboratory Data Acquisition and Experiments Control System. Technical Report TCRL-19, Turbomachinery Components Research Program, Department of Mechanical Engineering and Engineering Research Institute, Iowa State University, Ames, Iowa, 1980.
3. Fottner, L. Survey of Models for Shock and Shock/Boundary Layer Interaction Loss Prediction. To be published in AGARD/NATO report, Through-Flow Calculations in Turbomachines, 1981.
4. Schreiber, H. A. Untersuchung des geraden Verdichtergitters L030-4 bei schnallnahen Zuströmmachzahlen-Schaufelmittelschnitt des Transonikverdichterlaufrades 030. DFVLR IB 352-79/10, Oktober 1979.
5. Schäffler, A. Experimental and Analytical Investigation of the Effects of Reynolds Number and Blade Surface Roughness on Multistage Axial Flow Compressors. J. Eng. Power, Trans. ASME. 102: 5-13, 1980.
6. Koch, C. C. and L. H. Smith, Jr. Loss Sources and Magnitudes in Axial-Flow Compressors. J. Eng. Power, Trans. ASME. 98: 411-424, 1976. (Discussion by N. L. Sanger in J. Eng. Power, 99: 197, 1977).
7. Kluck, C. E. Prediction of Laminar-to-Turbulent Boundary Layer Transition in Axial-Flow Turbomachinery. Technical Report TCRL-21, Turbomachinery Components Research Program, Department of Mechanical Engineering and Engineering Research Institute, Iowa State University, Ames, Iowa, 1981.
8. Serovy, G. K. Deviation/Turning Angle Correlations. To be published in AGARD/NATO report Through-Flow Calculations in Turbomachines, 1981.

**Appendix A. EXPERIMENTAL DATA TABULATION AND REDUCTION
FOR PASSAGE TEST RIG (TASK I)**

Sample data tables representative of data collection by the data acquisition system and as stored in data files are shown in Figures A1-A5. A schematic of the passage test section showing the data coordinate system and traverse plane identification is given in Figure A6.

Currently, five different types of data files are collected and stored. The first of these files is made up of a line of five-hole probe data consisting of 12 items of raw collected data plus six additional reduced data parameters (see Figure A1). The six reduced parameters, shown at the right in the table, are the total pressure loss and static pressure coefficients along with the "q-dependent" velocity components and Mach number. These six values, whose formulation is discussed below, are stored as individual files on disk for later manipulation and plotting. The total 18 values (raw data plus reduced parameters) comprising the complete file are written out as they are collected on hard copy for permanent storage. Note that a single file or line in the table corresponds to one z (probe traverse) position for a given traverse plane, slide bar position, and passage or inlet boundary layer testing condition. These qualifiers on a particular data file are determined by a file directory label and file identification number. Thus in Figure A1, 21 files are listed in the table of data, each corresponding to one z-position from the upper endwall to the lower endwall. The complete table corresponds to one "pass" of the probe from one endwall to the other. The z-positions for the pass shown in Figure A1 are

SLIDE RATE POSITION 3.9%
 DATE 3/14/81
 ATMOSPHERIC PRESSURE 29.24 INHG
 PS(GAGE) -5.67 INHG

L-A FO	P5-FO	P1-FO	FO-ATM	YAW	T-BAR	T-PILEN	QC	PITCH	YM-YT	P1/00	Q/00	CPI	CFS	UX	UY	UZ	FPS	H*
INH20	INH20	INH20	DEG	DEG F	DEG R	DEG R	INH20	DEG	DEG R	DEG	DEG	DEG	DEG	DEG	DEG	DEG	FFS	--
-5.54	-5.67	-5.9	8.13	.96	71.5	544.	5.75	2.22	1.14	.729	1.25	.17	.1	139.	2.79	-5.43	.123	
-5.81	-5.56	-7.43	8.14	1.53	72.0	544.	5.75	.159	1.53	.763	1.28	.143	.094	143.	3.82	-3.97	.126	
-5.85	-5.49	-1.10	8.16	1.53	72.2	544.	5.75	.156	1.53	.705	1.22	.205	.09	137.	3.67	-3.75	.121	
-5.75	-5.65	-1.01	8.15	1.53	71.9	544.	5.75	.167	1.53	.723	1.24	.19	.087	139.	3.72	-4.05	.122	
-5.80	-5.64	-8.29	8.16	1.53	72.0	544.	5.75	.162	1.53	.755	1.27	.158	.087	142.	3.80	-4.02	.125	
-5.88	-5.51	-9.39	8.15	1.53	73.3	544.	5.75	.157	1.53	.733	1.25	.177	.09	140.	3.74	-3.83	.123	
-5.86	-5.46	-9.29	8.16	1.53	72.3	544.	5.75	.156	1.53	.731	1.25	.175	.093	140.	3.74	-3.81	.123	
-5.98	-5.54	-8.92	8.17	1.53	72.5	544.	5.75	.157	1.53	.742	1.26	.169	.089	141.	3.77	-3.88	.124	
-5.98	-5.43	-7.35	8.14	1.81	72.3	544.	5.75	.154	1.81	.767	1.28	.142	.092	143.	4.53	-3.85	.126	
-6.10	-5.34	-7.16	8.14	1.98	72.0	544.	5.75	.151	1.98	.772	1.29	.138	.089	143.	4.97	-3.79	.126	
-6.19	-5.25	-8.82	8.14	1.98	72.8	544.	5.75	.148	1.98	.752	1.26	.16	.087	142.	4.91	-3.68	.125	
-6.07	-5.20	-9.27	8.14	1.98	72.3	544.	5.75	.157	1.98	.776	1.25	.175	.099	139.	4.87	-3.62	.123	
-6.12	-5.29	-1.06	8.17	1.97	72.0	544.	5.75	.149	1.97	.716	1.23	.199	.085	138.	4.76	-3.61	.122	
-6.12	-5.34	-8.62	8.16	1.98	72.3	544.	5.75	.15	1.98	.754	1.26	.164	.085	141.	4.90	-3.72	.125	
-6.14	-5.31	-8.857	8.16	1.98	72.6	544.	5.75	.15	1.98	.751	1.26	.163	.086	141.	4.90	-3.71	.125	
-6.11	-5.33	-8.821	8.15	1.98	72.8	545.	5.75	.15	1.98	.756	1.27	.157	.088	142.	4.92	-3.74	.125	
-6.24	-5.31	-8.811	8.17	1.97	72.6	544.	5.75	.149	1.97	.763	1.27	.158	.079	143.	4.92	-3.71	.126	
-6.18	-5.34	-1.56	8.16	1.98	72.8	544.	5.75	.15	1.98	.757	1.26	.163	.081	142.	4.92	-3.72	.125	
-6.09	-5.35	-1.933	8.15	1.97	73.1	544.	5.75	.151	1.97	.738	1.25	.176	.086	140.	4.84	-3.7	.124	
-5.98	-5.37	-1.23	8.14	1.42	72.5	544.	5.75	.152	1.32	.684	1.2	.229	.087	135.	3.17	-3.59	.119	
-5.61	-5.42	-1.60	8.14	.25	73.7	545.	5.75	.159	.231	.603	1.13	.293	.104	127.	.514	-3.54	.112	

Fig. A1. Listing of five-hole probe data files.

1.25 in. (3.2 cm) to 8.25 in. (21 cm) by 3.5 in. (8.9 cm) increments, 8.75 in. (22.2 cm) to 14.75 in. (37.5 cm) by 0.50 in. (1.3 cm) increments, and 14.95 in. (38.0 cm) to 15.75 in. (40.0 cm) by 0.20 in. (0.51 cm) increments; the lower endwall is 16 in. from the top endwall.

The second type of data file, shown in Figure A2, consists of Kiel probe data and is similar in all aspects to the above file for the five-hole probe. Here four pieces of raw data are collected along with the reduced total pressure loss coefficient and q-dependent velocity. The entire field is written out on hard copy, with the 21 reduced total pressure loss coefficients for the entire "pass" being stored on disk as one data file. The Kiel data file is labeled by the slide bar position, traverse plane number, and passage testing condition in the hard copy heading. Figure A2 shows a table of data for one pass of the Kiel probe from upper endwall to lower endwall, with the same z-positions as for Figure A1.

The third, fourth, and fifth types of data files, shown in Figures A3, A4, and A5, represent total pressure loss and static pressure coefficients reduced from measured static tap pressures. Figure A3 lists the static and total pressure loss coefficient values for measured sidewall static taps. The numbers 9 through 16 refer to the static taps, where tap 9 is located 8.50 in. (21.6 cm) from the top endwall, tap 15 at 15.50 in. (39.4 cm) from the top endwall, and the rest spaced at 1 in. (2.54 cm) intervals. The letters S and P represent the suction and pressure sidewalls, respectively. The static pressure coefficients are all stored together in one data file on disk. These coefficients

SLIDE BAR POSITION -3.0%9F
 DATE 11/23/81
 ATMOSPHERIC PRESSURE 28.76 IN HG
 (PSO-PO) -8.05 IN H2O

P1-PO INH2O	P0-ATM INH2O	T-BAR DEG R	Q0	CPT	VEL FPS
-5.56	9.37	536	2.93	.151	108.
-6.36	9.38	536	2.93	.424	89.0
-8.22	9.39	536	2.93	1.05	28.0
-8.16	9.37	536	2.93	1.03	22.2
-7.82	9.40	536	2.93	.920	33.2
-6.56	9.38	536	2.93	.490	83.7
-6.46	9.39	536	2.93	.456	86.5
-6.47	9.37	536	2.93	.460	86.2
-6.34	9.38	536	2.93	.417	89.5
-6.13	9.35	536	2.93	.344	94.9
-5.95	9.39	536	2.93	.283	99.2
-5.82	9.39	536	2.93	.239	102.
-5.59	9.37	536	2.93	.160	107.
-5.49	9.39	536	2.93	.125	109.
-5.40	9.37	536	2.93	.096	111.
-5.44	9.38	536	2.93	.109	110.
-5.42	9.38	536	2.93	.104	111.
-5.52	9.37	536	2.93	.137	108.
-5.61	9.39	536	2.93	.167	107.
-5.76	9.36	536	2.93	.218	103.
-6.31	9.39	536	2.93	.404	90.5

Fig. A2. Listing of Kiel probe data files.

**SLIDE BAR9F
SIDEWALL STATICS**

Q0 2.736 (IN. H2O)

P0-ATM 8.978 (IN. H2O)

NO.	CFS	CPT
09S	-4640	2.475
10S	-4661	2.477
11S	-5301	2.541
12S	-5497	2.560
13S	-5021	2.513
14S	-4833	2.494
15S	-4569	2.468
16S	-4049	2.416
09P	-4882	2.499
10P	-4956	2.506
11P	-4641	2.475
12P	-4790	2.490
13P	-4666	2.477
14P	-1283	2.139
15P	0.1616	1.849
16P	0.0559	1.955

Fig. A3. Listing of reduced pressure coefficients for suction and pressure sidewalls.

**SLIDE BAR7F
BOTTOM ENDWALL STATICS**

X CPS CPT

-3.75	-.385	2.73
-3.00	-.401	2.74
-2.00	-.434	2.78
-1.00	-.444	2.79
0.000	-.446	2.79
1.000	-.441	2.78
2.000	-.433	2.78
3.000	-.436	2.78
3.750	-.423	2.77

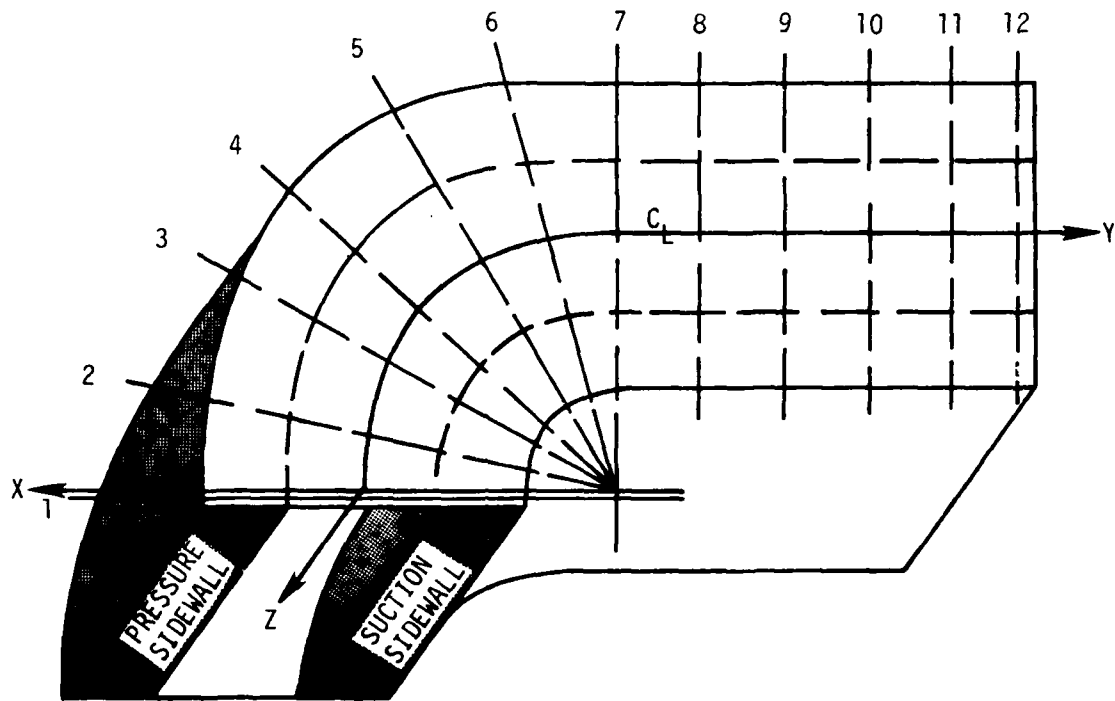
Fig. A4. Listing of reduced pressure coefficients for bottom endwall.

**SLIDE BAR12F
TOP ENDWALL STATICS**

X CPS CPT

-3.75	-.444	2.81
-3.00	-.446	2.81
-2.00	-.459	2.83
-1.00	-.458	2.82
0.000	-.460	2.82
1.000	-.454	2.82
2.000	-.456	2.82
3.000	-.441	2.81
3.750	-.458	2.82

Fig. A5. Listing of reduced pressure coefficients for top endwall.



TRaverse Plane No.	Y, INCHES(cm)	PASSAGE WIDTH INCHES, (cm)
1 (INLET)	-0.500 (-1.27)	9.00 (22.86)
2 (15 deg)	5.498 (13.97)	9.00 (22.86)
3 (30 deg)	10.996 (27.94)	8.80 (22.35)
4 (45 deg)	16.493 (41.89)	8.48 (21.54)
5 (60 deg)	21.991 (55.86)	8.00 (20.32)
6 (75 deg)	27.489 (69.82)	7.80 (19.81)
7 (90 deg)	32.987 (83.79)	7.80 (19.81)
8 (DISCHARGE)	38.487 (87.60)	7.75 (19.69)
9 (DISCHARGE)	43.987 (110.46)	7.75 (19.69)
10 (DISCHARGE)	49.487 (125.70)	7.75 (19.69)
11 (DISCHARGE)	54.487 (138.40)	7.75 (19.69)
12 (DISCHARGE)	60.487 (153.64)	7.75 (19.69)

Figure A6. Schematic of test section showing dimensions, traverse plane identification and coordinate system convention.

are stored in the cap order presented in the hard copy. No raw data are stored as hard copy or on disk for these last three tables.

The data listed in Figures A4 and A5 are measured and reduced exactly in the same manner as the data for Figure A3. Data of Figures A4 and A5 are for the bottom and top endwalls, respectively. The data as listed in Figures A4 and A5 are not stored on disk, but only on hard copy. Traverse plane number, inlet condition, and endwall label are printed in the table heading.

Definitions of measured and reduced data terms are as follows:

ATM	atmospheric (reference) pressure, in H_2O
P0	plenum (reference) pressure, in H_2O
P1,P4,P5	five-hole probe impact and pitch pressures
PBAR	barometric pressure, in Hg (abs)
PITCH	pitch angle (deg determined from probe calibration)
PS0	pitot static pressure, in H_2O (gage)
PT	total pressure, from probe calibration, in H_2O (gage)
Q	dynamic pressure, from probe calibration
Q0	pitot dynamic pressure, in H_2O
TBAR	atmospheric temperature, deg F
TPLEN	plenum temperature, deg F or deg R
VX	q-dependent x component of the flow velocity (ft/s)
VY	q-dependent y component of the flow velocity (ft/s)
VZ	q-dependent z component of the flow velocity (ft/s)
YAW	measured yaw angle (determined by probe null) from reference yaw for test section
YM-YT	yaw angle corrected for pitch (from probe calibration)

Data reductions from the tabulated data are as follows:

(1) Total pressure loss coefficient, C_{pt} , is defined as

$$C_{pt} = (p_{to} - p_t)/q_0$$

where p_t is total pressure, and p_{to} and q_0 are reference pitot total and dynamic pressures, respectively. Based on table entries, then,

$$CPT = 1 - (PT/Q0) + (PS0/Q0)$$

(2) Static pressure coefficient, C_{ps} , is defined as

$$C_{ps} = (p_s - p_{so})/q_0$$

where p_s is static pressure of the flow, and p_{so} and q_0 are the pitot static and dynamic pressures. Therefore,

$$CPS = (PT/Q0) - (Q/Q0) - (PS0/Q0)$$

(3) Flow velocity is determined from the measured q and density ρ_s according to

$$V = \sqrt{\frac{2q}{\rho_s}}$$

With the equation of state used to express ρ_s , the above expression becomes

$$V = \sqrt{\frac{2qRT_s}{p_s}}$$

where p_s and T_s are the pressure and temperature of the flow, respectively, and R the gas constant. The pressure p_s is in turn obtained from

$$p_s = [(PT/Q_0) - (Q/Q_0)](Q_0) + 13.6(\text{PBAR}), \text{ in H}_2\text{O (abs)}$$

Therefore, the expression for V, assuming $T_s = \text{TPLEN}$, and taking $R = 1716 \text{ ft}^2/\text{s}^2 \cdot ^\circ\text{F}$, becomes

$$V = 58.58 \sqrt{\frac{(Q/Q_0)(\text{TPLEN})}{(PT/Q_0) - (Q/Q_0) + 13.6(\text{PBAR}/Q_0)}}, \text{ ft/s}$$

(4) Since the acoustic velocity, c, is

$$c = \sqrt{kRT_s} = \sqrt{kR(\text{TPLEN})}$$

Mach number, $M = V/c$, is computed as

$$M = 1.20 \sqrt{\frac{(Q/Q_0)}{(PT/Q_0) - (Q/Q_0) + 13.6(\text{PBAR}/Q_0)}}$$

in which V from (3) above has been used, and the specific heat ratio, k, taken as 1.4.

(5) Flow velocity components are computed according to V from (3) above and the recorded pitch and corrected yaw angles as

$$VY = V / \sqrt{1 + \tan^2(\text{YAW}) + \tan^2(\text{PITCH})}$$

$$VX = VY \tan(\text{YAW})$$

$$VZ = VY \tan(\text{PITCH})$$

**APPENDIX B: EXPLANATION OF HOW FLOW PARAMETERS
DESCRIBING RESEARCH COMPRESSOR PER-
FORMANCE (TASK II) WERE OBTAINED**

1) Flow coefficient

$$\text{flow coefficient} = \phi = \frac{\text{cross-section-average axial velocity}}{\text{rotor blade tip velocity}} = \frac{\bar{V}_z}{U_t}$$

$$\text{where } \bar{V}_z = \frac{\text{venturi based mass flow rate}}{(\text{air density})(\text{cross-section area})} = \frac{\dot{m}_v}{\rho_{\text{air}} A}$$

$$\text{and } U_t = (\text{rotor blade tip radius})(\text{rotor angular velocity}) = r_t w$$

2) Head-rise coefficient

$$\text{head-rise coefficient} = \psi = \frac{\text{cross-section-average gage value of total head at second stage stator exit}}{U_t^2}$$

$$= \frac{\bar{H}_{2s}}{U_t^2}$$

where

$$\bar{H}_{2s} = \text{gage value of static head at second stage stator exit} + \frac{\bar{V}^2}{2}$$

$$\bar{H}_{2s} = h_{2s} + \frac{\bar{V}^2}{2}$$

and h_{2s} was determined with several static pressure taps in the second stage stator exit outer casing surface.

3) Work coefficient

$$\text{work coefficient} = \psi' = \frac{(\text{motor torque})(\omega)}{\dot{m}_v U_t^2}$$

$$\psi' = \frac{T\omega}{\dot{m}_v U_t^2}$$

where T is measured with the drive motor suspended on air journal bearings and a torque meter.

4) Efficiency

$$\text{efficiency} = \xi = \frac{\psi}{\psi'}$$

5) Local total head

$$\text{local total head} = H = \frac{[\text{manometer reading of total head}] [\text{specific weight of manometer fluid}]}{[\text{measured with total-head probe}] [\text{density of air}]}$$

$$H = \frac{H_{\text{mano}} \alpha_{\text{mano}}}{\rho_{\text{air}}}$$

6) Circumferential-mean total head

$$\text{circumferential-mean total head} = \bar{H} = \frac{1}{S} \int_0^S H dY$$

where S = blade-to-blade extent of measurement

Y = blade-to-blade direction coordinate

7) Local flow angle

local flow angle = β measured with a yaw probe

8) Circumferential-mean flow angle

$$\text{circumferential-mean flow angle} = \bar{\beta} = \frac{1}{S} \int_0^S \beta dY \text{ for rotor exit flows}$$

= approximate mean of freestream values of β only for stator exit flows since stator wake flow angle measurements were not attempted with the yaw probe

9) Local velocity

$$\text{local velocity} = V = \sqrt{2(H-h)}$$

10) Circumferential-mean velocity

$$\text{circumferential-mean velocity} = \bar{V} = \frac{1}{S} \int_0^S V dY$$

11) Circumferential-mean axial velocity

$$\text{circumferential-mean axial velocity} = \bar{V}_z = \bar{V} \cos \bar{\beta}$$

12) Stall limit

The stall limit was experimentally ascertained by noting at what flow coefficient (proceeding from higher to lower values of flow coefficient) the rotating stall condition could be audibly discerned. This procedure repeatedly produced a distinct stall limit flow coefficient.

APPENDIX C. NOTES ON RESEARCH VISIT TO DFVLR
(KÖLN) AND ONERA (CHATILLON),
21-30 September 1981

The objective of this visit to DFVLR and ONERA was to review experimental data originally made available by those organizations to AGARD Propulsion and Energetics Panel Working Group 12. These data were also used in the study of blade surface boundary layer development carried out as Task III of AFOSR Grant 81-0004.

Discussions were held with members of the research staff of the Institut für Antriebstechnik, Deutsche Forschungs- und Versuchsanstalt für Luft- und Raumfahrt. The major talks involved Dr.-Ing. H. Starken, Dr.-Ing. H. B. Weyer and Dr.-Ing. G. Winterfeld, the Director of the Institut.

At the Office National d'Etudes et de Recherches Aerospatiales, the principal discussion participants were Dr. G. Meauzé, J. Fabri and S. Boudigues, Directeur Scientifique of the Division de l'Energetique.

Technical Summary--DFVLR. During the past few years, two of the major research efforts at DFVLR have been parallel development of a dual-beam laser velocimeter method for flow field measurement in axial-flow compressor and turbines and the detailed aerodynamic study of a single-stage axial-flow compressor. As in most programs of this nature, parts of the aerodynamic investigation have been repeated as improvements in the measurement method have been made, and the measurement system has encountered difficulties due to compressor-related mechanical problems. The data of interest to us in our AFOSR work have been compressor rotor flow field survey measurements made at several flow

rates at 70 percent of design rotational speed. These data are of interest because on several blade-to-blade survey surfaces, upstream, intrablade and wake region measurements do not involve transonic flow conditions. We wanted to remove the complexities resulting from shock patterns in this phase of our work.

Although only one data point suitable for our work was delivered to AGARD WG-12, Weyer agreed to send the remaining 70 percent speed data to us and has now done so. In addition, questions arising in interpretation of the data were answered. Some points of clarification may be of use to others studying the DFVLR program.

The original DFVLR stage consisted of a rotor with MCA profile sections and a stator designed with NACA 65-series sections. Over a period of years, this stage was used extensively to generate aerodynamic data and to demonstrate and develop the capabilities of the laser measurement system. In our study of the data, we noticed that in the series of papers reporting this work, apparent differences existed in overall performance. In fact, there are three sets of overall performance data, and there appear to be two sets of laser data. The latest data have been supplied to us.

Starken has completed linear cascade investigations of three "cascade flow projection" profiles from the DFVLR rotor over a range of upstream Mach number and axial-velocity-density ratio. We consider this data to be extremely valuable and have the DFVLR internal reports for two sections.

Technical Summary--ONERA. French research on turbomachinery aerodynamics has been characterized by high quality flow visualization, extensive

development linear cascade testing techniques, and a long-term interest in unsteady flows.

One aspect of the ONERA cascade work during recent years has been the acquisition of detailed boundary layer development data on the suction surface of typical airfoil shapes. Meauzé has used these data to verify his computational work. Much of the ONERA work has received very limited distribution because of its proprietary nature.

Discussions with Meauzé and Fabri were related to the release of additional linear cascade boundary layer data and to a future ONERA test program on a "test case" cascade. There should be a standard set of cascade data, verified by tests in several linear cascade test rigs.

